A fungal endophyte-generated nucleoside signal regulates host cell death and promotes root colonization

Nick Dunken[1], Heidi Widmer[1], Gerd U. Balcke[2], Henryk Straube[3], Gregor Langen[1,4], Nyasha M. Charura[1], Pia Saake[1,4], Lisa Leson[1], Hanna Rövenich[1,4], Stephan Wawra[1,4], Armin Djamei[5], Alain Tissier[2], Claus-Peter Witte[3] and Alga Zuccaro[1,4*]

[1] University of Cologne, Institute for Plant Sciences, Cologne, Germany

[2] Department of Cell and Metabolic Biology, Institute of Plant Biochemistry, Halle (Saale), Germany

[3] Department of Molecular Nutrition and Biochemistry of Plants, Institute of Plant Nutrition, Leibniz University Hannover, Hannover, Germany

[4] Cluster of Excellence on Plant Sciences (CEPLAS)

[5] Department of Plant Pathology, Institute of Crop Science and Resource Conservation (INRES), University of Bonn, Bonn, Germany

[*] Corresponding author: azuccaro@uni-koeln.de

Summary

Intracellular colonization of plant roots by the beneficial fungal endophyte *Serendipita indica* follows a biphasic strategy. After an early biotrophic phase, the interaction switches to a host cell death phase restricted to the root epidermis and cortex layers. Host cell death contributes to successful fungal accommodation during beneficial interaction in *Arabidopsis thaliana*. How the host cell death is initiated and controlled is largely unknown. Here we show that two fungal enzymes, the ecto-5'-nucleotidase *Si*E5NT and the nuclease *Si*NucA, act synergistically in the plant apoplast at the onset of cell death to produce deoxyadenosine (dAdo), a potent cell death inducer in animal systems. Uptake of extracellular dAdo, but not of the structurally related adenosine (Ado), activates a previously undescribed cell death mechanism in *A. thaliana* and the basal land plant *Marchantia polymorpha*, suggesting a conserved cell death response to dAdo across land plant lineages. Mutation of the *A. thaliana* equilibrative nucleoside transporter *ENT3* confers resistance to extracellular dAdo-triggered cell death and leads to decreased fungal-mediated cell death during root colonization. A library screen of *A. thaliana* T-DNA insertion lines identified a nucleotide-binding leucine-rich repeat protein (NLR) as an additional intracellular component in dAdo-triggered cell death. Our data show that the combined activity of two apoplast-resident fungal enzymes leads to the production of a metabolite, which induces an NLR-modulated plant host cell death upon uptake.

In brief

Regulated host cell death is part of a plant defense strategy against pathogens but it is also involved in accommodating certain beneficial root microbes. We have identified extracellular metabolites and intracellular metabolic signals that contribute to beneficial root fungal endophyte colonization, and uncovered a conserved cell death mechanism likely co-opted for establishing plant-endophyte symbiosis.

Introduction

Regulated cell death occurs in plants as part of normal growth and development and in response to abiotic and biotic stimuli. In plant-microbe interactions, host cell death programs can mediate either resistance or successful infection. Depending on the type of microbial lifestyle (biotrophic or necrotrophic), host cell death can benefit the plant by stopping growth of biotrophs, or the microbe by promoting growth of necrotrophs. Thus, control of plant host cell death is vitally important for determining the outcome of an interaction. Several research lines indicate that controlled host cell death have a crucial role in certain beneficial interactions, challenging the paradigm that cell death in plant-microbe interactions implies pathogenesis or host-microbe incompatibility. Symbiosis with beneficial microbes, as well as infection by pathogens, requires a sophisticated control of host defence and nutrient fluxes. Certain features of beneficial microbes, such as the manipulation of host immunity, metabolism and host cell death, are reminiscent of pathogen infections. In *Rhizobium*-legume symbioses, root nodules are formed to provide a niche for bacterial nitrogen fixation. The formation of infection pockets in some of these symbioses is associated with host cell death and production of hydrogen peroxide (D'Haeze et al., 2003). Restricted cell death is also observed in ectomycorrhizal symbioses (Mucha et al., 2014; Ragnelli et al., 2014), and is required for the establishment of symbiotic interactions with the widely distributed beneficial fungi of the order Sebacinales (Deshmukh et al., 2006; Lahrmann et al., 2013; Qiang et al., 2012). Molecular environmental studies revealed that some of the most common taxa of this order display little, if any, host-specificity and interact with a large variety of plant species. Sebacinales isolates, including *Serendipita indica* and *S. vermifera*, exhibit beneficial effects such as growth promotion, increased seed production and pathogen protection, thereby playing a significant role in natural and managed ecosystems (Oberwinkler et al., 2013; Tedersoo et al., 2014; Weiss et al., 2016). A requirement for restricted host cell death in accommodation of certain beneficial microorganisms leads to the hypothesis that the activation of cell death mechanisms in roots have a more important ecological function than previously recognized.

In the hosts *Hordeum vulgare* (hereafter barley) and *Arabidopsis thaliana* (hereafter Arabidopsis), fungi of the order Sebacinales initially colonize living cells which die as the colonization proceeds (Deshmukh et al., 2006; Lahrmann et al., 2013; Lahrmann et al., 2015; Lahrmann and Zuccaro, 2012; Qiang et al., 2012; Zuccaro et al., 2011). This symbiosis-induced cell death is thought to contribute to niche differentiation during microbial competition for space and nutrients in the root and is restricted to colonized host cells in the epidermis and outer cortex. The host pathways controlling induction and execution of plant root cell death and the fungal elicitors/effectors that initiate this process in the roots remain

largely unknown (Lahrmann et al., 2013; Nizam et al., 2019; Qiang et al., 2012; Schneider and Lynch, 2018). Pathogenic and beneficial fungi have large repertoires of secreted effectors that can manipulate host cell physiology and suppress plant defence which promotes fungal colonization. In fungi, effectors are mainly described from biotrophic and hemibiotrophic leaf pathogens (Lo Presti et al., 2015). By contrast, only few effectors have been functionally characterized from root symbiotic fungi (Kloppholz et al., 2011; Nizam et al., 2019; Nostadt et al., 2020; Plett et al., 2014; Voß et al., 2018; Wawra et al., 2016). Therefore, the modes of action of mutualistic fungal effectors remain poorly understood.

Using genomics, transcriptomics and proteomics we identified *Serendipita indica* secreted proteins present in the root apoplast, the space outside the plasma membrane, including the cell walls, within which material can diffuse freely (Nizam et al., 2019). One secreted fungal protein consistently found at different symbiotic stages is the ecto-5'-nucleotidase *Si*E5NT (PIIN_01005) (Nizam et al., 2019). Expression of *E5NT* is induced during colonization of barley and Arabidopsis hosts, but not in fungal axenic culture (Nizam et al., 2019). Animal ecto-5'-nucleotidases play a key role in the conversion of AMP to adenosine, counteracting, the immunogenic effects of extracellular adenosine-5'-triphosphate (eATP) released from stimulated host cells (Antonioli et al., 2013). Extracellular ATP is another essential signalling molecule in plants where it regulates development and responses to biotic and abiotic stresses. In Arabidopsis, eATP mediates different cellular processes through its binding to the purinergic membrane-associated receptor proteins DORN1/P2K1 and recently described P2K2 (Pham et al., 2020). In the apoplast, ATP accumulation increases cytoplasmic calcium and induces a defence response against invading microbes. We have recently shown that perception of extracellular nucleotides, such as eATP, is important in plant-fungus interactions via colonization assays of the Arabidopsis *dorn1* knock out mutant that is better colonized by *S. indica*. *Si*E5NT is capable of hydrolysing ATP, ADP and AMP to adenosine and phosphate, altering eATP levels in the apoplast and plant responses to fungal colonization. Expression of extracellular *Si*E5NT in Arabidopsis leads to increased *S. indica* colonization, confirming its role as an apoplastic effector protein. Considering the important role *Si*E5NT plays in fungal accommodation at early symbiotic stages, we proposed that modulation of extracellular nucleotide levels and their perception play a key role in compatibility during early plant-fungus interactions in roots (Nizam et al., 2019). Secreted *Si*E5NT homologues are present also in fungal pathogens as *Colletotrichium incanum* and *Fusarium oxysporum* and other endophytes of Arabidopsis such as *C. tofieldiae* where their expression is induced during colonization, suggesting that extracellular purines-based biomolecules play a role also in other plant-fungus interactions.

At the onset of root cell death a small fungal endonuclease, which we named *Si*NucA (PIIN_02121), is secreted together with *Si*E5NT during barley and Arabidopsis colonization by *S. indica* (Nizam et al., 2019; Thürich et al., 2018). In plants, mechanisms linking immune sensing of DNA danger signals in the extracellular environment to innate pathways in the cytosol are poorly understood as the role of (deoxy)nucleotide metabolism in root colonization and cell-death. Here we show that the synergistic activity of *Si*NucA and *Si*E5NT leads to the production of deoxyadenosine (dAdo) and, in smaller amounts, other

118 deoxynucleosides from extracellular DNA (eDNA) that is released by the roots upon
119 microbial colonization in a process named root extracellular trap (RET) formation or by
120 microorganisms during biofilm development (Chambard et al., 2021; Driouich et al., 2019;
121 Tran et al., 2016; Wen et al., 2009). The production of dAdo by extracellular fungal enzymes
122 bears resemblance to *Staphylococcus aureus* dAdo-mediated immune cell death in
123 animals, which appears to ensure bacterial survival in host tissues (Thammavongsa et al.,
124 2013; Winstel et al., 2018). Staphylococcal nuclease and AdsA (a homologue of *S. indica*
125 E5NT) are both required to release dAdo from neutrophil extracellular traps (NETs) which
126 has a potent cytotoxic effect on macrophages and other immune cells (Thammavongsa et
127 al., 2013). Here we demonstrate that extracellular dAdo, but not the structurally similar Ado,
128 activates a previously unidentified cell death mechanism in Arabidopsis which induces cell
129 death marker gene expression, activates the 26S proteasome, increases electrolyte
130 leakage and decreases photosynthetic activity (F_V/F_M). Metabolomic analyses of exudates
131 of dAdo-treated or *S. indica*-colonized Arabidopsis roots showed extracellular accumulation
132 of the plant metabolite methylerythritol cyclodiphosphate (MEcPP), a precursor of plastidial
133 isoprenoids and a stress-specific retrograde signalling metabolite (Xiao et al., 2012).
134 Consistently, expression of either extracellular *Si*NucA or *Si*E5NT *in planta* increased
135 colonization by *S. indica* and host cell death. We found that mutation in the Arabidopsis
136 equilibrative nucleoside transporter 3 (ENT3) leads to a strong resistance phenotype to
137 dAdo-induced cell death but not to exposure to methyl jasmonate, a cell death inducer of
138 senescence. Congruently, the *ent3* KO Arabidopsis line displays less fungal-mediated cell
139 death in the root compared to *S. indica* colonized WT and accumulates less of the
140 extracellular signalling metabolite MEcPP in response to fungal colonization or dAdo
141 treatment. Finally, in a mutant screening of Arabidopsis T-DNA insertion lines, we found
142 that a previously uncharacterized Toll-like Interleukin 1 receptor (TIR) domain type NLR is
143 involved in dAdo-triggered cell death. We propose that modification of extracellular
144 metabolites by the activity of the fungal derived enzymes *Si*NucA and *Si*E5NT provides a
145 direct link between purine salvage, immunity and cell death in the roots.

146 **Results**

147 **Fading of host nuclei and vacuolar collapse are hallmarks of symbiotic cell death**
148 **during *S. indica* root colonization**

149 *S. indica* induces cell death in colonized root cells of Arabidopsis and barley resulting in
150 characteristic cytological features at later colonization stages. In these two hosts the timing
151 and extent of cell death differ (Lahrmann et al., 2013; Qiang et al., 2012). In Arabidopsis the
152 cell death phenotype is less prominent than in barley but cytological analyses revealed
153 fading of host nuclei, vacuolar collapse (Figure 1A-M) and endoplasmic reticulum (ER)
154 swelling in colonized cells (Qiang et al., 2012), indicative of ER-stress and host cell death
155 during root colonization. To characterize the timing of fungal-mediated root cell death, the
156 presence and shape of plant nuclei during the progression of *S. indica* colonization were
157 monitored by confocal laser scanning microscopy either by the use of the nucleic acid stain
158 DAPI (4',6-Diamidino-2'-phenylindole dihydrochloride) and the cell death stain SYTOX

159 Orange (Figure 1C-I) or by the use of an Arabidopsis line expressing the nuclear marker
160 H2B:mCherry (Figure 1A, B). Nuclei stained with SYTOX Orange were visible 7 to 8 days
161 post inoculation (dpi), indicating that at this time point Arabidopsis plasma and nuclear
162 membranes were permeable to the dye, a hallmark for cell death (Figure 1F, G). In the
163 Arabidopsis H2B:mCherry line the plant nuclei in the epidermal layer were often stretched,
164 faded and finally disappeared around 8 to 10 dpi in heavily colonized areas of the root
165 (Figure 1A, B). *S. indica* hyphae embedded within the plant nuclei in dying cells were
166 frequently observed, suggesting that the fungus can digest and feed on host nuclear DNA
167 (Figure 1C-E, H, I). The cytological analyses show that Arabidopsis root cell death starts
168 around 7 dpi and at 10 dpi most host nuclei have faded or disappeared in *S. indica* colonized
169 cells.

170 **_Si_NucA and _Si_E5NT act synergistically to produce deoxynucleosides**

171 Although the interaction between *S. indica* and plant roots has been studied in detail,
172 comparatively little is known about the contribution of apoplastic effectors to fungal
173 accommodation or the mechanism of cell death in this system (Nizam et al., 2019; Nostadt
174 et al., 2020; Rafiqi et al., 2013; Wawra et al., 2016). We therefore analysed soluble
175 apoplastic proteins in barley at different stages of *S. indica* colonization. We found that
176 *Si*E5NT was one of the predominant fungal proteins consistently present in this extracellular
177 compartment (Nizam et al., 2019). We previously showed that *Si*E5NT functions as a
178 membrane bound nucleotidase that is released to the apoplast during host colonization.
179 *Si*E5NT is capable of liberating phosphate and adenosine from ATP, ADP and AMP (Nizam
180 et al., 2019). Additionally, the small secreted protein *Si*NucA with predicted endonuclease
181 activity (Figure S1), was found in the apoplastic fluid of colonised barley roots at the onset
182 of cell death (5 dpi) (Nizam et al., 2019). *Si*NucA is also secreted during root colonization in
183 Arabidopsis (Thürich et al., 2018). Its expression is transiently induced during cell death in
184 barley and Arabidopsis compared to axenic fungal growth according to transcriptomic data
185 (Lahrmann et al., 2013) and quantitative PCR analyses (Figure 2A). This prompted us to
186 examine the involvement of this small secreted protein in fungal colonization and host cell
187 death in more detail. Secretion of *Si*NucA and its enzymatic activity were assessed by
188 overexpression of a *Si*NucA:HA:His construct in *S. indica* (Figure 2B, S2). Supernatants of
189 fungal OE strains, but not of the empty vector control strains, as well as the affinity purified
190 *Si*NucA were capable of degrading single and double-stranded DNA and RNA derived from
191 fungal and plant material, suggesting a non-specific nuclease activity (Figure 2C). Addition
192 of magnesium and calcium increased activity of *Si*NucA in *in vitro* assays whereas EDTA
193 inhibited it (Figure S3).

194 To explore the effects of *Si*NucA on colonization, we tested independent homozygous T3
195 lines heterologously expressing a native version of *Si*NucA in Arabidopsis under control of
196 the 35S promoter. As controls we used WT and segregating lines without *Si*NucA gene.
197 Expression of *Si*NucA in Arabidopsis led to higher fungal colonisation at 7 dpi, which
198 correlated with its expression level (Figure 2D, E), demonstrating its importance in fungal
199 accommodation. Localization studies by confocal microscopy imaging of Arabidopsis roots

200 expressing either full length *Si*NucA or a version without the N-terminal signal peptide (SP)
201 fused to mCherry confirmed secretion of the full-length mCherry-tagged *Si*NucA fusion
202 protein to the apoplast and functionality of the SP. After plasmolysis with 1M NaCl or
203 sorbitol, the mCherry fluorescence signal was visible at the cell walls for the full-length
204 *Si*NucA fusion protein and not for the cytoplasmic version without SP (Figure S4).
205 Remarkably, the presence of *S. indica* led to a re-localization of the full-length mCherry-
206 tagged *Si*NucA to the host nuclei only in cells colonized by the fungus and not in bystander
207 cells where the mCherry signal remained at the cell periphery also after plasmolysis (Figure
208 2F and S4, S5). The presence of *Si*NucA in the apoplast (Nizam et al., 2019) and in the
209 nucleus of colonized host cells (Figure 2F) suggests that this small secreted protein can be
210 redirected to the nucleus when produced by the fungus and can act on both eDNA and
211 nuclear DNA.

212 The co-occurrence of *Si*NucA and *Si*E5NT in the apoplast at 5 dpi led us to speculate that
213 these two enzymes might cooperate in promoting fungal colonization of roots. Using *Si*E5NT
214 affinity purified from leaves of *Nicotiana benthamiana*, which transiently expressed the
215 enzyme as secreted C-terminal Strep-tagged variant, we found activity with dAMP and AMP
216 whereas no activity was detected for any other deoxynucleotides (dGMP, dCMP, dTMP) or
217 ribonucleotides (GMP, UMP, 3′,5′-cAMP) tested. Moreover, dATP and the general
218 phosphatase substrate *para*-nitrophenyl pyrophosphate (pNPP) were not *Si*E5NT
219 substrates. Interestingly, only dAMP was hydrolysed at a constant rate whereas the AMP
220 hydrolysis rate gradually declined under the chosen reaction conditions (Figure S6A, B).
221 The Km for AMP (15.9 µM) was ~20-fold lower than for dAMP (361.6 µM) but the k_{cat} for
222 dAMP (11.9 s^{-1}) exceeded that of AMP (1.1 s^{-1}) by a factor of ~10 (Figure 3A, B). These
223 data suggest that *Si*E5NT hydrolyses AMP slightly better at low substrate concentrations
224 (below 20 µM) but is by far more efficient for dAMP at higher substrate concentrations which
225 might prevail in a nucleus undergoing degradation and in case of eDNA degradation. To
226 test the ability of *Si*NucA and *Si*E5NT to work together, we incubated DNA with *Si*E5NT and
227 *Si*NucA alone and in combination. As expected, *Si*NucA alone degraded DNA (Figure 3C)
228 but neither deoxynucleotides nor deoxynucleosides were detected as reaction products by
229 LC-MS analysis indicating that *Si*NucA degrades DNA to oligonucleotides. *Si*E5NT alone
230 also did not release deoxynucleotides from DNA but released small amounts of
231 deoxynucleosides (Figure 3D). However, in combination *Si*NucA and *Si*E5NT released
232 deoxynucleosides from DNA with a strong preference for dAdo, a potent cell death inducer
233 in animal systems. This demonstrates the ability of *Si*E5NT to use oligonucleotides released
234 by *Si*NucA as substrate and to act synergistically with *Si*NucA to preferentially release dAdo
235 from DNA (Figure S6C).

236 **dAdo induces cell death *in planta***

237 The production of dAdo and additional deoxynucleosides by the synergistic activity of the
238 two secreted fungal enzymes bears resemblance to *Staphylococcus aureus* dAdo-mediated
239 immune cell death in animal cells, which ensure the exclusion of macrophages from the
240 center of abscesses within which the bacteria survive (Thammavongsa et al., 2013; Winstel

241 et al., 2018). This motivated us to test the effect of dAdo *in planta*. Incubation of Arabidopsis
242 H2B-mCherry line with extracellular dAdo but not with Ado or buffer led to fading and
243 disappearance of nuclei in the roots within 48 hours (Figure 4A). This root cell death
244 phenotype was quantified via the use of the azo dye Evans Blue (Figure 4B, C).
245 Furthermore, extracellular dAdo triggered hallmarks of cell death such as increased
246 electrolyte leakage, induction of cell death marker gene expression as well as activation of
247 the 26S proteasome and decreased photosynthetic activity (F_V/F_M) (Figure 4D-H, S7). The
248 effects were concentration dependent and the removal of dAdo from the culture supernatant
249 24 hours after treatment led to recovery of Arabidopsis seedlings, suggesting that the
250 activation of the cell death program in Arabidopsis is still reversible at this stage (Figure S8,
251 S9).

252 A cell death phenotype was also observed in *N. benthamiana* young leaves during
253 expression via *Agrobacterium tumefaciens* infiltration of a *Si*E5NT construct with an N-
254 terminus signal peptide for secretion into the apoplastic space (Figure S10, S11) and in
255 seedlings incubated with dAdo (Figure S12). Cell death was not visible in older leaves or in
256 leaves of *N. benthamiana* expressing the control vector p19 or *Si*NucA alone. The observed
257 phenotype suggests that the presence of *Si*E5NT is sufficient to induce cell death in this
258 plant host upon wounding/damage by agroinfiltration which could release DNA and DNAses
259 into the apoplast or activate a response to the presence of the bacterium or its proteins
260 (Figure S10, S11). To test if dAdo-triggered cell death is conserved in basal plant lineages
261 we additionally tested its activity in the liverwort *Marchantia polymorpha*. Incubation with
262 dAdo led to cell death also in this plant species (Figure S13). Taken together, these data
263 indicate that the dAdo-mediated cell death mechanism is conserved across plant lineages.

264 **dAdo induces the MEP pathway and accumulation of the stress signal metabolite**
265 **MEcPP**

266 To investigate the mechanism by which dAdo induces and regulates cell death in plants and
267 if it activates stress signalling pathways, we analysed the transcriptional response of
268 Arabidopsis to this metabolite at 0, 3 and 12 hours, compared to a buffer control by RNA-
269 seq. Most marker genes for regulated cell death (Olvera-Carrillo et al., 2015) were
270 upregulated at 12 hours (Figure 4I & Table S1-3). Additionally, the plastidial 2-C-methyl-D-
271 erythritol 4-phosphate (MEP) pathway was induced upon incubation with dAdo at 12 hours
272 in Arabidopsis seedlings (Figure 4J & Table S4). Congruently, MEcPP a precursor of
273 plastidial isoprenoids and a stress-specific retrograde signalling metabolite produced by the
274 MEP pathway, accumulated extracellularly at 3 days post treatment (dpt) measured via LC-
275 MS/MS (Figure 4J). Abiotic stresses and wounding elevate the levels of cytoplasmic
276 MEcPP, which coordinates stress-response pathways *in planta* (Xiao et al., 2012).
277 Detection of this isoprenoid intermediate in the extracellular environment upon dAdo
278 treatment suggests that this metabolite may serve as a stress signal in bystander cells, a
279 putatively important function that needs to be further investigated. Incubation of Arabidopsis
280 with extracellular MEcPP did not lead to cell death, demonstrating that accumulation of this

281 metabolite is not sufficient to trigger cell death and therefore it is not the cause of the
282 observed dAdo-mediated cell death (Figure S14).

283 **dAdo-triggered signalling and cell death are not mediated by canonical pattern-**
284 **triggered immune responses**

285 To test if dAdo-triggered cell death is mediated by signalling generated by an extracellular
286 immune receptor, we tested the ability of this metabolite to induce a fast apoplastic response
287 by monitoring calcium influxes and ROS production. Both responses are part of PTI
288 (pattern-triggered immunity), a process activated by the recognition of MAMPs (microbe-
289 associated molecular patterns) or DAMPs (damage-associated molecular patterns) by
290 pattern-recognition receptors (PRRs) at the plasma membrane (Ngou et al., 2021; Yuan et
291 al., 2021; Zipfel and Oldroyd, 2017).

292 Incubation of Arabidopsis seedlings with dAdo did not elicit a calcium influx whereas
293 treatment with ATP or ADP, which have been previously described as DAMPs (Choi et al.
294 2014; Tanaka et al. 2014), or with dATP or dADP elicited a fast calcium influx dependent
295 on the extracellular ATP receptor DORN1 (Figure 5 A-C). Treatment with dAdo or with any
296 of the other purine derivatives did not trigger a ROS burst (Figure S15). On the other hand,
297 incubation with dAdo and to a lesser extent with ATP or dAMP, but not Ado, led to
298 accumulation of the marker metabolite MEcPP and the induction of the DAMP/MAMP and
299 fungal-responsive At1g58420 gene at 3 dpt (Figure 5D, E & Table S5) (Choi et al., 2014;
300 Kilian et al., 2007; Nizam et al., 2019). Collectively, these data indicate that dAdo does not
301 act as a typical extracellular DAMP or MAMP but induces a signalling pathway independent
302 of calcium influxes and ROS production.

303 **The *Arabidopsis* transporter ENT3 is required for dAdo-mediated signalling and cell**
304 **death**

305 The fact that we did not observe a canonical PTI response to dAdo let us speculate that
306 uptake of this metabolite is necessary to promote plant signalling and induce cell death. In
307 the animal system, treatment with extracellular dAdo causes accumulation of intracellular
308 dATP, which affects DNA synthesis and triggers apoptosis via caspase 3 activation (Winstel
309 et al., 2018). Rapidly dividing cells are particularly susceptible to dAdo-induced apoptosis
310 (Figure 4 A,B) and the toxic activity of dAdo in the animal system was shown to depend on
311 dAdo uptake by the human equilibrative nucleoside transporter 1 (hENT1) (Winstel et al.,
312 2018). *S. indica* was not sensitive to dAdo and displayed normal growth also at high
313 concentrations (Figure S16). In Arabidopsis, eight potential members of the ENT family are
314 annotated in the genome. Two are expressed in roots, the plasma membrane localized
315 ENT3 and the tonoplast localized ENT1. The *Arabidopsis ent3* knockout (KO) line displayed
316 a strong resistance phenotype to dAdo-induced cell death compared to WT and *ent1* KO,
317 but is not affected by methyl jasmonate-induced cell death (positive control) (Figure 6 A-C;
318 S17). *At*ENT3 was shown to transport adenosine and uridine with high affinity and to be
319 inhibited in competition assays by a number of different purine and pyrimidine nucleosides
320 and 2'-deoxynucleosides, including dAdo (Li et al., 2003). This indicates that *At*ENT3 has a

321 broad substrate specificity and is a strong candidate for the uptake of extracellular dAdo. In
322 a competition assay, addition of extracellular Ado reduced the cell death phenotype induced
323 by dAdo, suggesting that these two extracellular metabolites compete for the same
324 transporter at the cell membrane (Figure 6D). Interestingly, *ENT3* is more strongly
325 expressed in the epidermis compared to the rest of the root (Rich-Griffin et al., 2020),
326 suggesting that dAdo-induced cell death could display a certain level of cell type specificity.
327 This is in line with the root cell death phenotype observed after dAdo treatment with the
328 Evans Blue staining (Figure 4B, C). Together, these data demonstrate that a functional
329 ENT3 plays an important role in dAdo-triggered cell death in Arabidopsis most likely by
330 importing dAdo into the cytoplasm where it activates signalling resulting in cell death.
331 Congruently, the *ent3* KO line accumulates lower amounts of extracellular signalling
332 metabolites including MEcPP, GSSG and 3′,5′-cAMP in response to dAdo treatment at 3
333 dpt compared to the WT line (Figure 6E ,Table S6).

334 **Mutation of *At*ENT3 affects *S. indica*-mediated cell death and colonization**

335 Next, we determined whether *At*ENT3 plays a role in fungal accommodation and *S. indica*-
336 mediated cell death in roots. The *ent3* KO Arabidopsis line displayed significantly less cell
337 death upon colonization by *S. indica* compared to the WT line at 7, 10 and 14 dpi (Figure
338 6G, H). Furthermore, the *ent3* KO line was significantly less colonized by *S. indica* at 8 dpi
339 compared to the WT control as determined by quantitative reverse transcription PCR
340 (Figure 6I).

341 Upon *S. indica* colonization we observed a transient accumulation of the extracellular
342 signalling metabolites 3′,5′-cAMP at 3 dpi (early biotrophic phase) and MEcPP at 6 dpi
343 (onset of cell death). Additionally, a higher level of free phosphate at 10 dpi was observed
344 (Figure 6F, Table S6). In accordance with the decreased cell death phenotype in the *ent3*
345 KO line, the amount of these metabolites was lower upon *S. indica* colonization compared
346 to the WT line, indicating that the *Arabidopsis* ENT3 is important for fungal-mediated
347 signalling and cell death in this host. Modification of extracellular metabolites by the activity
348 of the fungal derived enzymes *Si*NucA and *Si*E5NT and the host transporter ENT3 provides,
349 for the first time, a direct link between purine salvage, immunity and cell death in roots. How
350 the metabolic status of the host affects fungal-induced cell death needs to be thoroughly
351 elucidated.

352 **An *At*NLR is involved in dAdo-mediated cell death**

353 To identify downstream genetic determinants associated with dAdo-mediated cell death *in*
354 *planta*, we performed a mutant screening of 6868 SALK Arabidopsis T-DNA insertion lines
355 (Figure S18). Sensitivity to dAdo was tested using Arabidopsis Col-0 WT as control and the
356 SALK mutant lines grown on solid media (1/2 MS) in 24-well plates with and without 500
357 µM dAdo for 14 days. The dAdo-insensitive lines (survivors) from the screening were
358 subsequently analysed using the PAM fluorometry in three independent biological
359 repetitions together with the Col-0 WT line as control. Thirteen lines with different degrees
360 of dAdo-resistance were identified (Table S7). One of the survivor SALK lines had a

361 mutation at the locus At5g45240 (SALK_034517) encoding a nucleotide binding, leucine-
362 rich repeat receptor (NLR). Mutation in this gene led to a reproducible and significant high
363 resistance to dAdo-induced cell death resulting in decreased electrolyte leakage and higher
364 photosynthetic activity compared to the wild type Col-0 upon incubation with dAdo (Figure
365 7 A-E). The NLR locus At5g45240 is directly adjacent to *RPS4* and *RRS1* and is part of a
366 bigger locus with several TIR-NLR (TNL) genes, which are not functionally characterized
367 (Figure S19). The involvement of an NLR suggests that dAdo-induced cell death is
368 regulated by the host immune response in plants rather than a consequence of cytoplasmic
369 toxicity as suggested for the animal cells.

370 **Discussion**

371 ***Symbiotic cell death: an evolutionary partially conserved mechanism?***

372 Root colonization by *S. indica* is associated with restricted host cell death. The mechanisms
373 behind the induction and regulation of this symbiotic cell death are poorly understood.
374 Earlier work showed that *S. indica* secretes E5NT, a ubiquitous fungal apoplastic enzyme
375 that catalyzes the conversion of adenosine nucleotides released by immune activated or
376 damaged host tissues to adenosine (Nizam et al., 2019). The implication of a secreted ecto-
377 5′-nucleotidase in host colonization resembles the mechanism evolved by *S. aureus* and
378 other animal pathogens to escape the host immune response by the secretion of AdsA that
379 converts eATP to Ado, a suppressor of immunity in animal cells (Thammavongsa et al.,
380 2009). In addition to the release of eATP by damaged animal cells, activated neutrophils
381 release NETs, extracellular matrices composed of nuclear and mitochondrial DNA armed
382 with granular proteins, cell-specific proteases, and antimicrobial peptides (Brinkmann et al.,
383 2004). NETs rapidly immobilize and kill bacterial pathogens (Driouich et al., 2019). *S.*
384 *aureus* escapes NETs by the secretion of proteases and the nuclease Nuc which degrade
385 antimicrobial peptides and DNA. Nuclease-mediated degradation of neutrophil NETs leads
386 to the formation of dAMP, which is converted by *S. aureus* AdsA into dAdo. Macrophages
387 and other immune cells are highly sensitive to dAdo intoxication. This cellular intoxication is
388 mediated by uptake via equilibrative nucleoside transporters (Thammavongsa et al., 2013;
389 Winstel et al., 2018). The *S. aureus* escape mechanism is based on the cooperative work
390 of two extracellular microbial enzymes and enables staphylococcus to block phagocyte
391 infiltration of abscess lesions and bacterial clearance. Similar to neutrophils, plant roots
392 secret RETs, root extracellular traps made of extracellular DNA and a variety of
393 antimicrobial compounds and polysaccharides. RETs and NETs exhibit similar
394 compositional and functional properties but unlike the NETs, RETs production is not solely
395 induced upon microbial infection but RETs are released continuously during root
396 development to form a large mucilage-rich network in the rhizosphere (Chambard et al.,
397 2021; Driouich et al., 2019; Hawes et al., 2016; Tran et al., 2016). *S. indica* is able to grow
398 within RETs and along the root tip (Figure S20) and to digest extracellular DNA via the
399 secretion of the nuclease NucA which accumulates in the root apoplast at the onset of cell
400 death (Nizam et al., 2019). Here, we show that the combined enzymatic activity of *Si*E5NT
401 and *Si*NucA, concomitantly present in the apoplast, catalyses the conversion of

402 deoxyadenosine nucleotides derived by nuclease digestion of extracellular DNA to
403 deoxyadenosine. Most importantly, we demonstrate that uptake via *At*ENT3 of
404 deoxyadenosine is required for host cell death in the roots. Mutation of ENT3 leads to
405 decreased cell death and impaired colonization by *S. indica*, substantiating the importance
406 of extracellular nucleosides uptake in modulating fungal accommodation and cell death. The
407 identification of a previously unknown immune-metabolic axis by which cells respond to
408 extracellular purine nucleosides and trigger cell death in plants suggests a certain
409 conservation or functional convergence between the immune evasion and escape
410 mechanisms evolved by *S. aureus* and other bacterial pathogens of animals and dAdo-
411 triggered cell death during plant-fungal endophyte interaction in the roots.

412 To ward off infections by microbial pathogens, plants have evolved immune receptors that
413 are essential for mounting a successful defense response. Plasma membrane localized
414 PRRs are able to perceive conserved MAMPs/DAMPs and induce a relatively mild PTI
415 immune response. Successful plant-associated microbes can deliver suites of effectors to
416 dampen PTI for successful host colonization. In turn, plants have evolved polymorphic
417 intracellular resistance (R) proteins to detect the presence and/or activity of the effectors,
418 which results in a robust defense response termed effector-triggered immunity (ETI) which
419 potentiate PTI (Ngou et al., 2021; Yuan et al., 2021). The majority of R proteins belong to
420 the nucleotide-binding (NB) leucine-rich repeat (LRR) (NLR) family, which is further
421 classified as Toll-like Interleukin 1 receptor (TIR) type NLRs (TNLs) or coiled-coil type NLRs
422 (CNLs) based on their N-terminal domains (Wu et al., 2019). TNLs generally act as sensors
423 of microbial effectors, while several CNLs are called helper NLRs and signal downstream
424 of many sensor NLRs in Arabidopsis (Saur et al., 2021; Wu et al., 2019). The implication of
425 a TNL in resistance to dAdo-mediated cell death in Arabidopsis suggest that this NLR could
426 be guarding a protein that is targeted by dAdo. Alternatively, it is possible that dAdo converts
427 into a plausible substrate of TNLs related to either nicotinamide adenine dinucleotide (NAD)
428 or to 2′,3′-cAMP, a noncanonical cyclic nucleotide monophosphate (cNMP) (Horsefield et
429 al., 2019; Wan et al., 2019; Yu et al., 2021). Plant TIR domains of NLRs are enzymes
430 capable of degrading NAD in its oxidized form (NAD^+). The TIR domain NADase function is
431 necessary but insufficient to activate plant immune responses. Recently, it was shown that
432 plant TIR proteins, besides being NADases, act as 2′,3′-cAMP/cGMP synthetases by
433 hydrolyzing RNA/DNA. Mutations specifically disrupting the synthetase activity abrogate
434 TIR-mediated cell death in *N. benthamiana*, supporting an important role for these cNMPs
435 in TIR signalling (Yu et al., 2021). Accumulation of extracellular 3′,5′-cAMP upon *S. indica*
436 colonization and dAdo treatment establish a link with cyclic nucleotide monophosphates.
437 Further analysis needs to be done in order to characterize the metabolism of dAdo inside
438 plant cells and how intracellular dAdo leads to activation of the TNL in Arabidopsis. As TIR
439 domain type NLRs are also present in animals, our findings open opportunities for further
440 study the implication of TNLs in dAdo-triggered cell death in plants and beyond.

441 In the animal systems, it was shown that after import of dAdo into macrophages, dAdo-
442 mediated toxicity involves conversion of dAdo to dAMP by the activity of deoxycytidine
443 kinase (DCK) and adenosine kinase (ADK) and signalling via subsequent conversion into

444 the corresponding di- and tri-phosphates by nucleotide kinases and activation of caspase-
445 3-induced apoptosis (Winstel et al., 2018). The absence of caspases in plants and the
446 implication of an NLR in dAdo-mediated cell death in Arabidopsis, strongly suggest that this
447 part of the pathway is not conserved between plants and animals and rely on different
448 regulation and execution mechanisms that need to be further studied.

449 In conclusion, we uncovered a cellular signalling pathway that responds to extracellular
450 DNA–derived metabolites, coupling extracellular nucleoside transport by an equilibrative
451 nucleoside transporter to cellular activation of the MEP pathway and cell death regulated
452 by an NLR. The fact that dAdo triggers cell death in different plant species, including a basal
453 one, suggests that this pathway is likely conserved and may represent an ancient cell death
454 mechanism that is co-opted for establishing plant-endophyte symbiosis. This paves the way
455 for a better understanding of immunometabolism in plant-microbe interactions.

456 **Material and Methods**

457 **Fungal strains and culturing techniques**

458 *S. indica* strain DSM11827 (Deutsche Sammlung von Mikroorganismen und Zellkulturen,
459 Braunschweig, Germany) was grown on complete medium (CM) with 2% (w/v) glucose and
460 1.5 % (w/v) agar as described before in (Hilbert et al., 2012). Liquid (CM) cultures were
461 incubated from spores at 28 °C & 120 rpm.

462 **Plant lines and Arabidopsis transformation**

463 Seeds of the *A. thaliana* ecotype Columbia 0 (Col-0), Col-0^{AEQ} and Col-0^{AEQ} *dorn1* (Choi et
464 al. 2014), SALK lines SALK_034517 (*nlr*) and SALK_204257(*ent3*) were used in the context
465 of the experiments. Additionally, Col-0 expressing histone H2B fused to mCherry
466 (H2B:2xmCherry) under the UBQ10 promoter in root cells (Marquès-Bueno et al., 2016)
467 were used in this study. Col-0 transformation was performed by the floral dip method as
468 described in (Nizam et al., 2019) to create the transgenic lines *35S::SiNucA* and
469 *35S::SiNucA:mCherry* (with and without signal peptide).

470 For *Marchantia polymorpha*, gemmae of male Tak1 and female Tak2 gametophyte were
471 used.

472 **Plant growth conditions and fungal inoculation**

473 Surface-sterilized seeds were germinated and grown on ½ MS medium (Murashige-Skoog-
474 Medium, with vitamins, pH 5.7) with 1 % (w/v) sucrose and 0.4 % (w/v) Gelrite under short
475 day conditions (8 h light, 16 h dark) with 130 µmol m^{-2} s^{-1} of light and 22 °C/18 °C.
476 For fungal inoculation, 7-day-old seedlings were transferred to ½ MS or $1/10$ PNM (Plant
477 Nutrion Medium, pH 5.7) plates without sucrose (15-20 seedlings per plate). 1 ml water
478 containing $5x10^5$ *S. indica* chlamydospores was pipetted on the root and the surrounding
479 area. Control plants were inoculated with sterile water.

480 For harvesting, single roots were thoroughly washed with water, a 4 cm long root part
481 starting 0.5 cm below the shoot cut and immediately frozen in liquid nitrogen. Two to three
482 plates of 20 seedlings each were pooled per replicate.

483 **Confocal microscopy**

484 Colonized Arabidopsis roots were stained with 5 µg/ml Wheat Germ Agglutinin Alexa Fluor
485 488 conjugate (WGA-AF 488, Life Technologies, Thermo Fisher Scientific, Schwerte,
486 Germany) or 1 µM FGB1-FITC from (Wawra et al., 2019) to visualize the fungal cell wall.
487 250 ng/ml 4',6-Diamidino-2'-phenylindole dihydrochloride (DAPI) or 500 nM SYTOX Orange
488 (Life Technologies, Thermo Fisher Scientific, Schwerte, Germany) were used as nucleic
489 acid stains.

490 For live cell confocal laser scanning microscopy, a TCS SP8 confocal microscope (Leica,
491 Wetzlar, Germany) was used. Excitation of AF 488 and FITC was done with an argon laser
492 at 488 nm and the emitted light was detected with a hybrid detector at 500-550 nm. mCherry
493 and SYTOX orange were excited with a DPSS laser at 561 nm and the signal was detected
494 with a hybrid detector at 590-660 nm. DAPI was excited with a diode laser at 405 nm and
495 the emitted light was detected with a hybrid detector at 415-460 nm.

496 **DNA & RNA extraction**

497 DNA was extracted from frozen root or fungal material as described in Wawra et al. 2016.
498 In short, ca. 500 mg ground frozen material was dissolved in 1 ml CTAB extraction buffer
499 (100 mM TrisHCl pH 7.5, 50 mM EDTA pH 8, 1.5 M NaCl, 2 % (w/v)
500 Cetyltrimethylammonium bromide, 0.05 % (v/v) ß- mercaptoethanol) and homogenized for
501 10 min. 500 µl of chloroform:isoamylalcohol mixture (24:1) was added and the tubes were
502 mixed for 5 min and centrifuged. Ethanol and 1 volume chloroform:isoamylalcohol mixture
503 (24:1) were added to the upper phase and centrifuged again. The DNA in the upper phase
504 was precipitated with 1 volume isopropanol at 4 °C for 1 h.

505 RNA was extracted with TRIzol (Invitrogen, Thermo Fisher Scientific, Schwerte, Germany)
506 and DNA digested with DNase I (Thermo Fisher Scientific, Schwerte, Germany) according
507 to manufacturer's instructions. cDNA was synthesized using the Fermentas First Strand
508 cDNA Synthesis Kit (Thermo Fisher Scientific, Schwerte, Germany).

509 **Quantitative RT-PCR analysis**

510 For quantitative real-time PCR the 2x GoTaq qPCR master mix (Promega, Mannheim,
511 Germany) was used. 500 nM primer forward and reverse each and 10-20 ng template cDNA
512 or gDNA were added. The reaction was running in a CFX connect real time system (BioRad,
513 Munich, Germany) with the following program: 95°C 3min, 95°C 15s, 59°C 20s, 72°C 30s,
514 40 cycles and melting curve analysis. Relative expression was calculated using the $2^{-\Delta\Delta CT}$
515 method (Livak and Schmittgen 2001). All used Oligonucleotides can be found in Table S8.

516 ***Serendipita indica* transformation**
517 *S. indica* protoplasts were transformed by the PEG-mediated transformation system as
518 described in (Wawra et al., 2019).

519 **Nuclease activity assay**

520 To test nuclease activity of the purified protein, 10 nM *Si*NUCA were mixed with 100 ng
521 linearized plasmid, 1 µg gDNA or 1 µg RNA in buffer (5 mM Tris pH 8, 1 mM $MgCl_2$, 1 mM
522 $CaCl_2$, 0.1 % microelement solution (from CM medium)). The mixture was incubated for 1
523 to 30 min at RT, loading dye was added and the samples run on a 1-2 % agarose gel.

524 To test nuclease activity in *S. indica* culture filtrate, a 5-day-old CM culture was crushed and
525 incubated for another 3 days. The culture was filtered through Miracloth (Millipore Merck,
526 Darmstadt, Germany) and 50 µl culture filtrate were added to linearized plasmid DNA, gDNA
527 or RNA.

528 ***Si*NucA-HA-His purification**

529 A 7-day-old liquid culture of *S. indica* grown in CM medium was filtered through Miracloth.
530 The mycelium was washed with 0.9 % NaCl and crushed in a blender (MicrotronR MB550
531 homogenizer (Kinematica, Luzern, Switzerland)) in fresh CM medium. The culture was
532 regenerated for two days. Subsequently, the culture was filtered with Miracloth and through
533 a 0.45 µm membrane filter. To this cell-free culture filtrate 1 mM Phenylmethanesulfonyl
534 fluoride (PMSF) was added and the pH was adjusted to pH 7 with 1 M Tris pH 8. The
535 proteins were precipitated using 80 % ammonium sulfate. The protein pellet was
536 resuspended in 20 mM Tris pH 8. The proteins were separated by size exclusion
537 chromatography (Sephadex G 200 column, Hiload 6/600) usinga 20 mM Tris pH 8 / 150
538 mM NaCl buffer. Fractions containing *Si*NucA-HA-His were desalted by dialysis and
539 checked by SDS-PAGE and anti-HA western blot. The protein was stored in 20 mM Tris pH
540 8. Identity of the protein was checked by LC-MS/MS.

541 **Protein purification and measurement of enzymatic kinetics of *Si*E5NTs**

542 *Si*E5NT fused to a C-terminal haemaglutinin (HA) and Strep tag (pXCScpmv-HAStrep, V69)
543 was transiently expressed in *Nicotiana benthaminana* and purified by affinity
544 chromatography as described by (Myrach et al., 2017; Werner et al., 2008). Enzyme
545 concentrations were determined using bovine serum albumin standards after SDS-PAGE
546 and Coomassie staining employing an Odyssey Fc dual mode imaging system (Li-cor
547 Biosciences, Germany).

548 To determine the substrate specificity, different substrates were tested. Briefly, 10 µl purified
549 enzyme (1.9 x 10^{-4} mg protein) were added to 70 µl reaction buffer (10 mM MES buffer, pH
550 6.0; 1 mM $CaCl_2$ and 1 mM $MgCl_2$) and pre-incubated for 5 min. Substrates were added (20
551 µl of a 5 mM stock solution) reaching a final reaction volume of 100 µl. The reaction was
552 quenched with 400 µl MeOH at the indicated time points and centrifuged for 10 min at

553 21.000*g* at 4°C. The supernatant was evaporated in a vacuum concentrator and the dry
554 pellet resuspended in 100 µl HPLC mobile phase A.

555 The samples were analyzed on an Agilent 1200 SL HPLC system equipped with a diode
556 array detector. 10 µl of the sample was injected onto a Supelcosil LC–18–T column (Sigma-
557 Aldrich) with a flowrate of 0.8 ml min^{-1} and a column temperature of 25°C. The analytes
558 were separated by the following gradient: 0 min, 100% A; 9 min, 100% A; 15 min, 75% A;
559 17.5 min, 10% A; 19 min, 0% A; 23 min, 0% A; 24 min, 100% A; 30 min, 100% A. The mobile
560 phase A consisted of 100 mM KH_2PO_4, pH 6.0, in deionized water and the mobile phase B
561 consisted of 90% 100 mM KH_2PO_4, pH 6.0, in deionized water and 10% MeOH. Respective
562 standard solutions were used for quantification. The data were analyzed using the Agilent
563 Chemstation software.

564 The kinetic constants for deoxyadenosine monophosphate and adenosine monophosphate
565 were determined using the EnzCheck (Thermo Fisher Scientific, Waltham, USA)
566 phosphatase assay kit according to specifications but using only one tenth of the
567 recommended reaction volume.

568 **Release of deoxynucleosides from salmon sperm DNA by *Si*NucA and *Si*E5NT**

569 10 µg Salmon sperm DNA were incubated with 4 µl *Si*NucA, 10 µl *Si*E5NT or a combination
570 of both in a final volume of 40 µl containing 10 mM HEPES, pH 7.2; 100 mM $MgCl_2$ and 1
571 mM DTT. Before adding the DNA, the enzymes were incubated for 5 min in the buffer
572 mixture. The reaction was incubated at 22°C for 1 h and inactivated at 95°C for 5 min
573 followed by centrifugation for 20 min at 40000*g* and 4°C. 20 µl of the supernatant were
574 analyzed on a 2% agarose gel. The remaining 20 µl of the supernatant were mixed with 50
575 µl water and used for HPLC MS/MS analysis. Samples and standards were analyzed using
576 an Agilent 1290 Infinity II HPLC System coupled with an Agilent 6470 triple quadrupole
577 mass spectrometer. Analytes (10 µl samples) were separated on a 50 x 4.6 mm Polaris
578 C18A column (Agilent) using the following gradient: 0 min, 96% A; 8 min, 35% A; 8.2 min,
579 0% A; 10 min, 0% A; 10.1 min, 96% A. Mobile phase A consisted of 10 mM ammonium
580 acetate, pH 7.5, and mobile phase B was pure MeOH. The flow rate was 0.6 ml min^{-1} and
581 the column temperature was 30°C. The in-source parameters were set as described
582 previously for deoxyribonucleoside analysis (Straube et al., 2021). All analytes were
583 measured in positive mode. Transitions (precursor ions and product ions), collision energies
584 and fragmentor energies are listed in Table S9.

585 **PAM fluorometric measurements**

586 The measurements of PAM fluorometry were performed by transferring 9-day-old
587 Arabidopsis seedlings into 24 well plates containing 2 ml of 2.5 mM MES buffer (pH 5.6). 3
588 seedlings were pooled into one well. After 24 h of regeneration, the seedlings were treated
589 with solutions of 5' deoxyadenosine (dAdo), adenosine (Ado) or methyljasmonate (all
590 Sigma-Aldrich, Taufkirchen, Germany), adjusting to an end concentration of 500 µM. The
591 treated seedlings were incubated for 20 minutes in total darkness to reach a dark-adapted

592 state. The photosynthetic activity of the plants was measured using the M-Series PAM
593 fluorometer (Heinz Walz GmbH, Effeltrich, Germany). The data was evaluated using the
594 ImagingWin software (v.2.41a; Walz, Germany). If further analysis of the development of
595 photosynthetic area was required, it was evaluated with Fiji (ImageJ).

596 **Cell death staining with Evans Blue**

597 A modified protocol as described in (Vijayaraghavareddy et al., 2017)was used.To quantify
598 *S. indica* induced cell death in *Arabidopsis*, plants were used for cell death staining at three
599 time points, 7, 10 and 14 days post fungal spore inoculation, using five plants per treatment.
600 For dAdo (or chemically induced cell death) induced cell death, plants were used for
601 microscopy after 4 days of cell death treatment. To remove external fungal growth or
602 chemical treatment solutions, plants were washed three times in ddH_2O before cell death
603 staining in a 2.5mM Evans Blue solution (Sigma-Aldrich, Lot #MKCH7958), dissolved in
604 0.1M $CaCl_2$ pH 5.6 for 15 minutes. After extensive washing for one hour with ddH_2O, images
605 were obtained using a Leica M165 FC microscope.

606 **Activity-based protein profiling**

607 After they were treated with 500 µM dAdo, 500 µM Ado or MES buffer, 9-day-old
608 Arabidopsis seedlings were frozen in liquid nitrogen, ground and resolved in 50 mM Tris-
609 HCl buffer (pH 7). After centrifugation, the supernatant was split and either treated with the
610 proteasome inhibitor MG132 (end concentration: 50 µM, Company) or DMSO for 30
611 minutes. The samples were then incubated with the 26S proteasome probe MVB072 (end
612 concentration: 1 µM, (Kolodziejek et al., 2010) for 2 h. Afterwards, the samples were
613 denaturated at 95°C in SDS loading dye and separated on 12 % SDS gels. The probe was
614 visualized using the rhodamine settings (excitiation: 532 nm, emission: 580 nm) on a
615 ChemiDoc (BioRad, CA, USA). The protein content of the samples were visualized by
616 staining the gel with SYPRO™Ruby (Invitrogen, Carlsbad, CA,USA) according to the
617 manufacturer's instructions.

618 **RNA seq**

619 7-day-old seedlings were transferred from plates to individual wells of 24-well plates
620 containing 0.5 mL liquid ½ MS medium supplemented with 0.5% (w/v) sucrose. Following 5
621 additional days in liquid culture, the medium was replaced with 1 mL 500 µM dAdo in 2.5
622 mM MES buffer pH 5.6, or 2.5 mM MES buffer pH 5.6 alone as negative control. Three
623 replicates of four seedlings each were harvested for each treatment at 0, 3, and 12 hours
624 post treatment (hpt), snap-frozen in liquid nitrogen and stored at -80°C until processing for
625 RNA extraction. Total RNA was extracted using the TRIZOL reagent as described above.
626 RNA integrity was confirmed by gel electrophoresis and quantity and purity were determined
627 using a NanoDrop 2000. Stranded mRNA-seq Libraries were prepared according to the
628 manufacturer's instructions (Vazyme Biotech Co., Nanjing, China). Qualified libraries were
629 sequenced on a HiSeq 3000 system instrument at Genomics & Transcriptomics Laboratory,
630 Heinrich-Heine University, Germany, to generate >100 million reads with a 150 bp read

631 length from three biological replicates. Trimmomatic (v. 0.36,(Bolger et al., 2014)) was used
632 for quality trimming and adapter clipping and reads were then mapped to the *Arabidopsis*
633 *thaliana* TAIR10 CDS assembly and quantified using kallisto (v. 0.46.2,(Bray et al., 2016)),
634 which resulted in estimated counts and transcripts per million (TPM) values. The log2 fold
635 difference of the gene expression between conditions was calculated using R packages
636 tximport (Soneson et al., 2015) and DESeq2 (Love et al., 2014). Genes with statistical
637 significance were selected (FDR adjusted p value < 0.05). Data are deposited to the NCBI
638 under the BioProject accession number xxxx.

639 **Collection of extracellular fluid**

640 7-day-old Arabidopsis seedlings, germinated on ½ MS agar with 1 % sucrose were
641 transferred into 24 well plates. Each well contained 3 seedlings in 1.5 ml 2.5 mM MES and
642 the specific treatment. After transfer the plants were returned to the growth chamber for
643 three days. The seedlings were then removed and the liquid was centrifuged at 4000 g for
644 15 minutes. The supernatant was lyophilized and sent for metabolite analysis.

645 **Metabolite analysis**

646 5 µl of apoplastic fluid were injected to an Acquity UPLC (Waters Inc.) equipped with a
647 Nucleoshell RP18 column (Macherey & Nagel, 150mm x 2 mm x 2.1µm) using
648 tributylammonium as ion pairing agent. Solvent A: 10 mM tributylamine (aqueous) acidified
649 with glacial acetic acid to pH 6.2; solvent B acetonitrile. Gradient: 0-2 min: 2% B, 2-18 min
650 2-36% B, 18-21 min 36-95% B, 21-22.5 min 95% B, 22.51-24 min 2% B. The column flow
651 was 0.4 ml min^{-1} throughout. The column temperature was 40 °C. Scheduled multiple
652 reaction monitoring (MRM)-based metabolite detection was performed in negative mode
653 electrospray ionization (ESI) on a QTrap 6500 (AB-Sciex GmbH, Darmstadt, Germany: ion
654 source gas 1: 60 psi, ion source gas 2: 70 psi, curtain gas: 35 psi, temperature: 450 °C, Ion
655 spray voltage floating: and -4500V). MRM transitions were of 189 metabolites covering the
656 central carbon and energy metabolism were previously signal-optimized and retention times
657 were determined (Table S10).

658 **Ca^{2+} influx quantification**

659 Calcium influx assays were performed as previously described in (Wanke et al. 2020). In
660 brief, single 7-day-old Arabidopsis seedlings were placed into white 96-well plates filled with
661 200 µl reconstitution buffer (2.5 mM MES pH 5.7 [Sigma-Aldrich, Taufkirchen, Germany],
662 10 mM $CaCl_2$ [Roth, Karlsruhe, Germany]). Before overnight incubation in the dark, the
663 solution was replaced with 133 µl reconstitution buffer containing 10 mM coelenterazine
664 (Roth, Karlsruhe, Germany). On the following day, chemiluminescence was measured
665 using a TECAN SPARK 10M microplate plate reader. After the baseline measurement, 67
666 µl of three-fold concentrated elicitor solutions (or Milli-Q-water as a mock control) was
667 manually added. Cytosolic calcium influx upon elicitor addition was constantly measured for
668 30 min. In order to assess undischarged aequorin for treatment normalization, 100 µl of 3

669 M $CaCl_2$ (in 30% EtOH) was injected into each well, followed by constant measurement for
670 1 min. All steps were performed with an integration time of 450 msec.

671 **Heterologous protein production in *Nicotiana benthamiana* and protein purification**
672

673 For heterologous protein production in *Nicotiana benthamiana, l*eaves of 4-week-old plants
674 were infiltrated with *Agrobacterium tumefaciens* GV3101 strains. *A. tumefaciens* were
675 grown for 2 days in LB liquid medium with the appropriate antibiotics at 28°C, 180 rpm until
676 an OD_{600} of 1 was reached. The cultures were centrifuged at 3500 rpm for 15 min at RT,
677 supernatant was discarded and resuspended in 1 ml infiltration buffer (10 mM MES pH 5.5,
678 10 mM $MgCl_2$, 200 µM Acetosyringone) and incubated for 1 h in the dark at 28°C, 180 rpm.
679 All strains were diluted to OD_{600} of 1 using the infiltration buffer. Each strain was mixed with
680 P19-expressing strains in a 1:1 ratio. 2-3 leaves were infiltrated per plant using a needleless
681 syringe. At 4 dpi, the leaves were detached from the plant and ground in liquid nitrogen.
682 The protein purification was performed according to (Werner et al., 2008) including minor
683 modifications: a 15 ml tube was filled up to the 2 ml mark with grinded leaf material and 2
684 ml cold extraction buffer (100 mM Tris pH 8.0, 100 mM NaCl, 5 mM EDTA, 0.5 % Triton
685 X100, 10 mM DTT, 100 µg/ml Avidin) was added. The powder was re-suspended by
686 vortexing and subsequently centrifuged at 12000 rpm and 4°C for 10 min. Supernatant was
687 transferred to a new tube and 100 µl Strep-Tactin® Macroprep (50% slurry) was added and
688 incubated for 60 minutes at 4°C in a rotation wheel. The mixture was centrifuged for 30 s at
689 700xg at RT and the supernatant was removed completely from the beads. The beads were
690 washed once with 4 ml and 2 more times with 2 ml washing buffer (50 mM Tris pH 8.0, 100
691 mM NaCl, 0.5 mM EDTA, 0.005 % Triton X-100, 2 mM DTT) by centrifugation for 30 s at
692 700xg, and discarding the supernatant. During the last wash, the beads were transferred
693 into a 1.5 ml low-binding tube. The beads were either directly boiled for 5 min at 95°C with
694 6x SDS loading dye to run on a SDS PAGE or the proteins were eluted from the beads by
695 adding 100 µl elution buffer (wash buffer + 2.5 – 10 mM biotin) and incubation at 25 °C,
696 >800 rpm for 5 min. The samples were centrifuged for 20 s at 700xg and elution was
697 repeated. Elution fractions were pooled, SDS loading dye was added and samples were run
698 on a SDS PAGE followed by a Western Blot.

699 **Ion leakage measurements**

700 The measurements of ion leakage were prepared identically like the seedlings for PAM
701 fluorometry measurements. The ion leakage was measured using a conductivity meter
702 (LAQUAtwin EC-11; Horiba, Newhampton,UK).

703 **Oxidative burst assay**

704 Individual 7-day-old Arabidopsis seedlings were transferred into white 96-well plates
705 containing 200 µl reconstitution buffer (2.5 mM MES pH 5.7 (Sigma-Aldrich, Taufkirchen,
706 Germany), 10 mM $CaCl_2$ (Roth, Karlsruhe, Germany) and incubated overnight in the growth
707 chamber. The following day, the buffer was exchanged with 133 µl of reconstitution
708 supplemented with 15 µg ml^{-1} horseradish peroxidase (Sigma-Aldrich, Taufkirchen,

709 Germany) and 15 µM L-O12 (Wako Chemicals, Neuss, Germany). Following 10 min
710 incubation, 67 µL of three-fold concentrated elicitor solutions (or Milli-Q water as a mock
711 control) was manually added to the wells. Measurements were started immediately and
712 chemiluminescence was constantly measured with an integration time of 450 msec using a
713 TECAN SPARK 10M microplate reader (Tecan, Männedorf, Switzerland).

714 **Acknowledgments**

715 We would like to thanks Prof. Jane Parker for discussions and for reading the manuscript
716 prior submission. ND & AZ also want to thank Lisa Madhi and Lucia Schmitz for their
717 excellent support in the laboratory. ND was supported by the Max-Planck-Gesellschaft
718 through the International Max Planck Research School (IMPRS) on 'Understanding
719 Complex Plant Traits using Computational and Evolutionary Approaches' and the University
720 of Cologne. AZ acknowledges support from the Cluster of Excellence on Plant Sciences
721 (CEPLAS) funded by the Deutsche Forschungsgemeinschaft (DFG, German Research
722 Foundation) under Germany's Excellence Strategy – EXC 2048/1 – Project ID: 390686111
723 and the SFB project ID: 1403–414786233. CPW acknowledges support from DFG grant
724 WI3411/8-1. Graphical illustrations were designed with the BioRender online tool.

725 References

726 Antonioli, L., Pacher, P., Vizi, E.S., and Hasko, G. (2013). CD39 and CD73 in immunity and
727 inflammation. Trends in Molecular Medicine *19*, 355-367.
728 Bolger, A.M., Lohse, M., and Usadel, B. (2014). Trimmomatic: a flexible trimmer for Illumina
729 sequence data. Bioinformatics *30*, 2114-2120.
730 Bray, N.L., Pimentel, H., Melsted, P., and Pachter, L. (2016). Near-optimal probabilistic RNA-seq
731 quantification. Nature biotechnology *34*, 525-527.
732 Brinkmann, V., Reichard, U., Goosmann, C., Fauler, B., Uhlemann, Y., Weiss, D.S., Weinrauch,
733 Y., and Zychlinsky, A. (2004). Neutrophil extracellular traps kill bacteria. Science *303*, 1532-1535.
734 Chambard, M., Plasson, C., Derambure, C., Coutant, S., Tournier, I., Lefranc, B., Leprince, J.M.,
735 Kiefer-Meyer, M.C., Driouich, A., Follet-Gueye, M.L.*, et al.* (2021). New Insights into Plant
736 Extracellular DNA. A Study in Soybean Root Extracellular Trap. Cells *10*.
737 Choi, J., Tanaka, K., Cao, Y., Qi, Y., Qiu, J., Liang, Y., Lee, S.Y., and Stacey, G. (2014).
738 Identification of a plant receptor for extracellular ATP. Science *343*, 290-294.
739 D'Haeze, W., De Rycke, R., Mathis, R., Goormachtig, S., Pagnotta, S., Verplancke, C., Capoen,
740 W., and Holsters, M. (2003). Reactive oxygen species and ethylene play a positive role in lateral
741 root base nodulation of a semiaquatic legume. Proceedings of the National Academy of Sciences
742 *100*, 11789-11794.
743 Deshmukh, S., Huckelhoven, R., Schafer, P., Imani, J., Sharma, M., Weiss, M., Waller, F., and
744 Kogel, K.H. (2006). The root endophytic fungus Piriformospora indica requires host cell death for
745 proliferation during mutualistic symbiosis with barley. Proc Natl Acad Sci U S A *103*, 18450-18457.
746 Driouich, A., Smith, C., Ropitaux, M., Chambard, M., Boulogne, I., Bernard, S., Follet-Gueye, M.L.,
747 Vicre, M., and Moore, J. (2019). Root extracellular traps versus neutrophil extracellular traps in
748 host defence, a case of functional convergence? Biol Rev Camb Philos Soc *94*, 1685-1700.
749 Hawes, M., Allen, C., Turgeon, B.G., Curlango-Rivera, G., Tran, T.M., Huskey, D.A., and Xiong,
750 Z.G. (2016). Root Border Cells and Their Role in Plant Defense. Annu Rev Phytopathol *54*, 143-
751 161.
752 Hilbert, M., Voll, L.M., Ding, Y., Hofmann, J., Sharma, M., and Zuccaro, A. (2012). Indole
753 derivative production by the root endophyte Piriformospora indica is not required for growth
754 promotion but for biotrophic colonization of barley roots. New Phytologist *196*, 520-534.

755 Horsefield, S., Burdett, H., Zhang, X., Manik, M.K., Shi, Y., Chen, J., Qi, T., Gilley, J., Lai, J.S.,
756 Rank, M.X., *et al.* (2019). NAD(+) cleavage activity by animal and plant TIR domains in cell death
757 pathways. Science *365*, 793-799.
758 Kilian, J., Whitehead, D., Horak, J., Wanke, D., Weinl, S., Batistic, O., D'Angelo, C., Bornberg-
759 Bauer, E., Kudla, J., and Harter, K. (2007). The AtGenExpress global stress expression data set:
760 protocols, evaluation and model data analysis of UV-B light, drought and cold stress responses.
761 The Plant Journal *50*, 347-363.
762 Kloppholz, S., Kuhn, H., and Requena, N. (2011). A Secreted Fungal Effector of Glomus
763 intraradices Promotes Symbiotic Biotrophy. Curr Biol *21*, 1204-1209.
764 Kolodziejek, I., Misas-Villamil, J.C., Kaschani, F., Clerc, J., Gu, C., Krahn, D., Niessen, S.,
765 Verdoes, M., Willems, L.I., Overkleeft, H.S., *et al.* (2010). Proteasome Activity Imaging and
766 Profiling Characterizes Bacterial Effector Syringolin A Plant Physiology *155*, 477-489.
767 Lahrmann, U., Ding, Y., Banhara, A., Rath, M., Hajirezaei, M.R., Doehlemann, S., von Wiren, N.,
768 Parniske, M., and Zuccaro, A. (2013). Host-related metabolic cues affect colonization strategies of
769 a root endophyte. Proceedings of the National Academy of Sciences of the United States of
770 America *110*, 13965-13970.
771 Lahrmann, U., Strehmel, N., Langen, G., Frerigmann, H., Leson, L., Ding, Y., Scheel, D., Herklotz,
772 S., Hilbert, M., and Zuccaro, A. (2015). Mutualistic root endophytism is not associated with the
773 reduction of saprotrophic traits and requires a noncompromised plant innate immunity. New
774 Phytologist *207*, 841-857.
775 Lahrmann, U., and Zuccaro, A. (2012). Opprimo ergo sum-Evasion and Suppression in the Root
776 Endophytic Fungus Piriformospora indica. Molecular Plant-Microbe Interactions *25*, 727-737.
777 Li, G., Liu, K., Baldwin, S.A., and Wang, D. (2003). Equilibrative nucleoside transporters of
778 Arabidopsis thaliana. cDNA cloning, expression pattern, and analysis of transport activities. The
779 Journal of biological chemistry *278*, 35732-35742.
780 Lo Presti, L., Lanver, D., Schweizer, G., Tanaka, S., Liang, L., Tollot, M., Zuccaro, A., Reissmann,
781 S., Kahmann, R., and Merchant, S. (2015). Fungal Effectors and Plant Susceptibility. In Annual
782 Review of Plant Biology, Vol 66, pp. 513-545.
783 Love, M.I., Huber, W., and Anders, S. (2014). Moderated estimation of fold change and dispersion
784 for RNA-seq data with DESeq2. Genome biology *15*, 550.
785 Marquès-Bueno, M.M., Morao, A.K., Cayrel, A., Platre, M.P., Barberon, M., Caillieux, E., Colot, V.,
786 Jaillais, Y., Roudier, F., and Vert, G. (2016). A versatile Multisite Gateway-compatible promoter
787 and transgenic line collection for cell type-specific functional genomics in Arabidopsis. The Plant
788 Journal *85*, 320-333.
789 Mucha, J., Guzicka, M., Ratajczak, E., and Zadworny, M. (2014). Strategies utilized by trophically
790 diverse fungal species for Pinus sylvestris root colonization. Tree Physiol *34*, 73-86.
791 Myrach, T., Zhu, A., and Witte, C.P. (2017). The assembly of the plant urease activation complex
792 and the essential role of the urease accessory protein G (UreG) in delivery of nickel to urease. The
793 Journal of biological chemistry *292*, 14556-14565.
794 Ngou, B.P.M., Ahn, H.K., Ding, P., and Jones, J.D.G. (2021). Mutual potentiation of plant immunity
795 by cell-surface and intracellular receptors. Nature *592*, 110-115.
796 Nizam, S., Qiang, X., Wawra, S., Nostadt, R., Getzke, F., Schwanke, F., Dreyer, I., Langen, G.,
797 and Zuccaro, A. (2019). Serendipita indica E5'NT modulates extracellular nucleotide levels in the
798 plant apoplast and affects fungal colonization. EMBO Rep *20*.
799 Nostadt, R., Hilbert, M., Nizam, S., Rovenich, H., Wawra, S., Martin, J., Kupper, H., Mijovilovich,
800 A., Ursinus, A., Langen, G., *et al.* (2020). A secreted fungal histidine- and alanine-rich protein
801 regulates metal ion homeostasis and oxidative stress. New Phytol.
802 Oberwinkler, F., Riess, K., Bauer, R., Selosse, M.-A., Weiß, M., Garnica, S., and Zuccaro, A.
803 (2013). Enigmatic Sebacinales. Mycological Progress *12*, 1-27.
804 Olvera-Carrillo, Y., Van Bel, M., Van Hautegem, T., Fendrych, M., Huysmans, M., Simaskova, M.,
805 van Durme, M., Buscaill, P., Rivas, S., Coll, N.S., *et al.* (2015). A Conserved Core of Programmed
806 Cell Death Indicator Genes Discriminates Developmentally and Environmentally Induced
807 Programmed Cell Death in Plants. Plant Physiol *169*, 2684-2699.

808 Pham, A.Q., Cho, S.-H., Nguyen, C.T., and Stacey, G. (2020). Arabidopsis Lectin Receptor Kinase
809 P2K2 Is a Second Plant Receptor for Extracellular ATP and Contributes to Innate
810 Immunity1 [OPEN]. Plant Physiology *183*, 1364-1375.
811 Plett, J.M., Daguerre, Y., Wittulsky, S., Vayssieres, A., Deveau, A., Melton, S.J., Kohler, A.,
812 Morrell-Falvey, J.L., Brun, A., Veneault-Fourrey, C.*, et al.* (2014). Effector MiSSP7 of the
813 mutualistic fungus Laccaria bicolor stabilizes the Populus JAZ6 protein and represses jasmonic
814 acid (JA) responsive genes. Proc Natl Acad Sci U S A *111*, 8299-8304.
815 Qiang, X., Zechmann, B., Reitz, M.U., Kogel, K.H., and Schafer, P. (2012). The mutualistic fungus
816 Piriformospora indica colonizes Arabidopsis roots by inducing an endoplasmic reticulum stress-
817 triggered caspase-dependent cell death. Plant Cell *24*, 794-809.
818 Rafiqi, M., Jelonek, L., Akum, N.F., Zhang, F., and Kogel, K.H. (2013). Effector candidates in the
819 secretome of Piriformospora indica, a ubiquitous plant-associated fungus. Front Plant Sci *4*, 228.
820 Ragnelli, A.M., Aimola, P., Maione, M., Zarivi, O., Leonardi, M., and Pacioni, G. (2014). The cell
821 death phenomenon during Tuber ectomycorrhiza morphogenesis. Plant Biosystems - An
822 International Journal Dealing with all Aspects of Plant Biology *148*, 473-482.
823 Rich-Griffin, C., Stechemesser, A., Finch, J., Lucas, E., Ott, S., and Schäfer, P. (2020). Single-Cell
824 Transcriptomics: A High-Resolution Avenue for Plant Functional Genomics. Trends in plant
825 science *25*, 186-197.
826 Saur, I.M.L., Panstruga, R., and Schulze-Lefert, P. (2021). NOD-like receptor-mediated plant
827 immunity: from structure to cell death. Nat Rev Immunol *21*, 305-318.
828 Schneider, H.M., and Lynch, J.P. (2018). Functional implications of root cortical senescence for
829 soil resource capture. Plant and Soil *423*, 13-26.
830 Soneson, C., Love, M.I., and Robinson, M.D. (2015). Differential analyses for RNA-seq: transcript-
831 level estimates improve gene-level inferences. F1000Research *4*, 1521.
832 Straube, H., Niehaus, M., Zwittian, S., Witte, C.P., and Herde, M. (2021). Enhanced nucleotide
833 analysis enables the quantification of deoxynucleotides in plants and algae revealing connections
834 between nucleoside and deoxynucleoside metabolism. Plant Cell *33*, 270-289.
835 Tedersoo, L., Bahram, M., Ryberg, M., Otsing, E., Koljalg, U., and Abarenkov, K. (2014). Global
836 biogeography of the ectomycorrhizal /sebacina lineage (Fungi, Sebacinales) as revealed from
837 comparative phylogenetics analyses. Mol Ecol.
838 Thammavongsa, V., Kern, J.W., Missiakas, D.M., and Schneewind, O. (2009). Staphylococcus
839 aureus synthesizes adenosine to escape host immune responses. J Exp Med *206*, 2417-2427.
840 Thammavongsa, V., Missiakas, D.M., and Schneewind, O. (2013). Staphylococcus aureus
841 degrades neutrophil extracellular traps to promote immune cell death. Science *342*, 863-866.
842 Thürich, J., Meichsner, D., Furch, A.C.U., Pfalz, J., Krüger, T., Kniemeyer, O., Brakhage, A., and
843 Oelmüller, R. (2018). Arabidopsis thaliana responds to colonisation of Piriformospora indica by
844 secretion of symbiosis-specific proteins. PLOS ONE *13*, e0209658.
845 Tran, T.M., MacIntyre, A., Hawes, M., and Allen, C. (2016). Escaping Underground Nets:
846 Extracellular DNases Degrade Plant Extracellular Traps and Contribute to Virulence of the Plant
847 Pathogenic Bacterium Ralstonia solanacearum. PLoS Pathog *12*, e1005686.
848 Vijayaraghavareddy, P., Adhinarayanreddy, V., Vemanna, R.S., Sreeman, S., and Makarla, U.
849 (2017). Quantification of Membrane Damage/Cell Death Using Evan's Blue Staining Technique.
850 Bio-protocol *7*, e2519.
851 Voß, S., Betz, R., Heidt, S., Corradi, N., and Requena, N. (2018). RiCRN1, a Crinkler Effector
852 From the Arbuscular Mycorrhizal Fungus Rhizophagus irregularis, Functions in Arbuscule
853 Development. Frontiers in Microbiology *9*.
854 Wan, L., Essuman, K., Anderson, R.G., Sasaki, Y., Monteiro, F., Chung, E.H., Osborne Nishimura,
855 E., DiAntonio, A., Milbrandt, J., Dangl, J.L.*, et al.* (2019). TIR domains of plant immune receptors
856 are NAD(+)-cleaving enzymes that promote cell death. Science *365*, 799-803.
857 Wawra, S., Fesel, P., Widmer, H., Neumann, U., Lahrmann, U., Becker, S., Hehemann, J.H.,
858 Langen, G., and Zuccaro, A. (2019). FGB1 and WSC3 are in planta-induced beta-glucan-binding
859 fungal lectins with different functions. New Phytol.
860 Wawra, S., Fesel, P., Widmer, H., Timm, M., Seibel, J., Leson, L., Kesseler, L., Nostadt, R.,
861 Hilbert, M., Langen, G.*, et al.* (2016). The fungal-specific beta-glucan-binding lectin FGB1 alters
862 cell-wall composition and suppresses glucan-triggered immunity in plants. Nat Commun *7*, 13188.

863 Weiss, M., Waller, F., Zuccaro, A., and Selosse, M.A. (2016). Sebacinales - one thousand and one
864 interactions with land plants. New Phytologist *211*, 20-40.
865 Wen, F.S., White, G.J., VanEtten, H.D., Xiong, Z.G., and Hawes, M.C. (2009). Extracellular DNA
866 Is Required for Root Tip Resistance to Fungal Infection. Plant Physiology *151*, 820-829.
867 Werner, A.K., Sparkes, I.A., Romeis, T., and Witte, C.P. (2008). Identification, biochemical
868 characterization, and subcellular localization of allantoate amidohydrolases from Arabidopsis and
869 soybean. Plant Physiol *146*, 418-430.
870 Winstel, V., Missiakas, D., and Schneewind, O. (2018). Staphylococcus aureus targets the purine
871 salvage pathway to kill phagocytes. Proc Natl Acad Sci U S A *115*, 6846-6851.
872 Wu, Z., Li, M., Dong, O.X., Xia, S., Liang, W., Bao, Y., Wasteneys, G., and Li, X. (2019).
873 Differential regulation of TNL-mediated immune signaling by redundant helper CNLs. New Phytol
874 *222*, 938-953.
875 Xiao, Y., Savchenko, T., Baidoo, E.E., Chehab, W.E., Hayden, D.M., Tolstikov, V., Corwin, J.A.,
876 Kliebenstein, D.J., Keasling, J.D., and Dehesh, K. (2012). Retrograde signaling by the plastidial
877 metabolite MEcPP regulates expression of nuclear stress-response genes. Cell *149*, 1525-1535.
878 Yu, D., Song, W., Tan, E.Y.J., Liu, L., Cao, Y., Jirschitzka, J., Li, E., Logemann, E., Xu, C., Huang,
879 S.*, et al.* (2021). TIR domains of plant immune receptors are 2′,3′-cAMP/cGMP synthetases
880 mediating cell death. bioRxiv, 2021.2011.2009.467869.
881 Yuan, M., Jiang, Z., Bi, G., Nomura, K., Liu, M., Wang, Y., Cai, B., Zhou, J.M., He, S.Y., and Xin,
882 X.F. (2021). Pattern-recognition receptors are required for NLR-mediated plant immunity. Nature
883 *592*, 105-109.
884 Zipfel, C., and Oldroyd, G.E.D. (2017). Plant signalling in symbiosis and immunity. Nature *543*,
885 328-336.
886 Zuccaro, A., Lahrmann, U., Gueldener, U., Langen, G., Pfiffi, S., Biedenkopf, D., Wong, P.,
887 Samans, B., Grimm, C., Basiewicz, M.*, et al.* (2011). Endophytic Life Strategies Decoded by
888 Genome and Transcriptome Analyses of the Mutualistic Root Symbiont Piriformospora indica. Plos
889 Pathogens *7*.

890

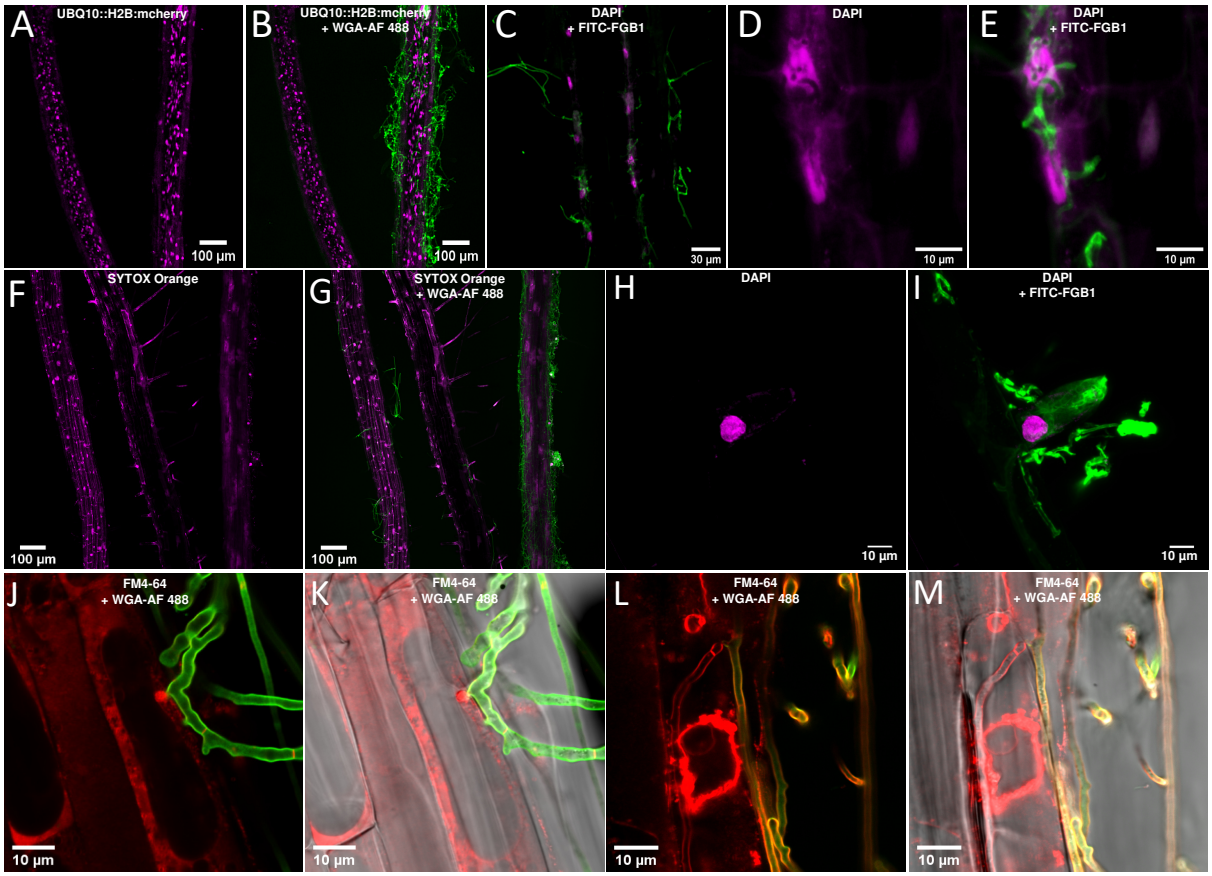

Figure 1. Host cell death during *S. indica* root colonization

(A and B) Arabidopsis roots expressing the fluorescent nuclei marker UBQ10::H2B:mCherry (magenta) and stained with the fungal cell wall marker Alexa Fluor dye WGA-AF 488 (green) at 10 dpi.
(C) Plant nuclei stained with DAPI (magenta) and fungal cell wall and matrix stained with the β-glucan binding lectin FGB1-FITC 488 (green) at 6dpi. With progression of *S. indica* colonization host nuclei often get stretched and fade.
(D and E) Close up of *S. indica* hyphae embedded in a host nucleus from (C).
(F and G) Staining of nucleic acids of *S. indica*-colonized roots with the dead-cell indicator (membrane integrity marker) SYTOX Orange (magenta) and fungal hyphae using WGA-AF 488 (green) at 10 dpi.
(H and I) *S. indica* hyphae fluorescently labelled with the β-glucan binding lectin FGB1-FITC 488 (green), embedded in a DAPI-stained host nucleus (magenta) at 6dpi.
(J-M) Progression of vacuolar collapse of colonized root cells. Fungal hyphae are stained using WGA-AF 488 (green) while membranes are stained with FM4-64 (red).
(J and K) Initial biotrophic colonization.
(L and M) vacuolar collapse in a dying host cell.
CLSM was repeated at least five times using 3 to 4 *S. indica* colonized plants. Fading of nuclei at the onset of cell death during fungal colonization was observed regularly.

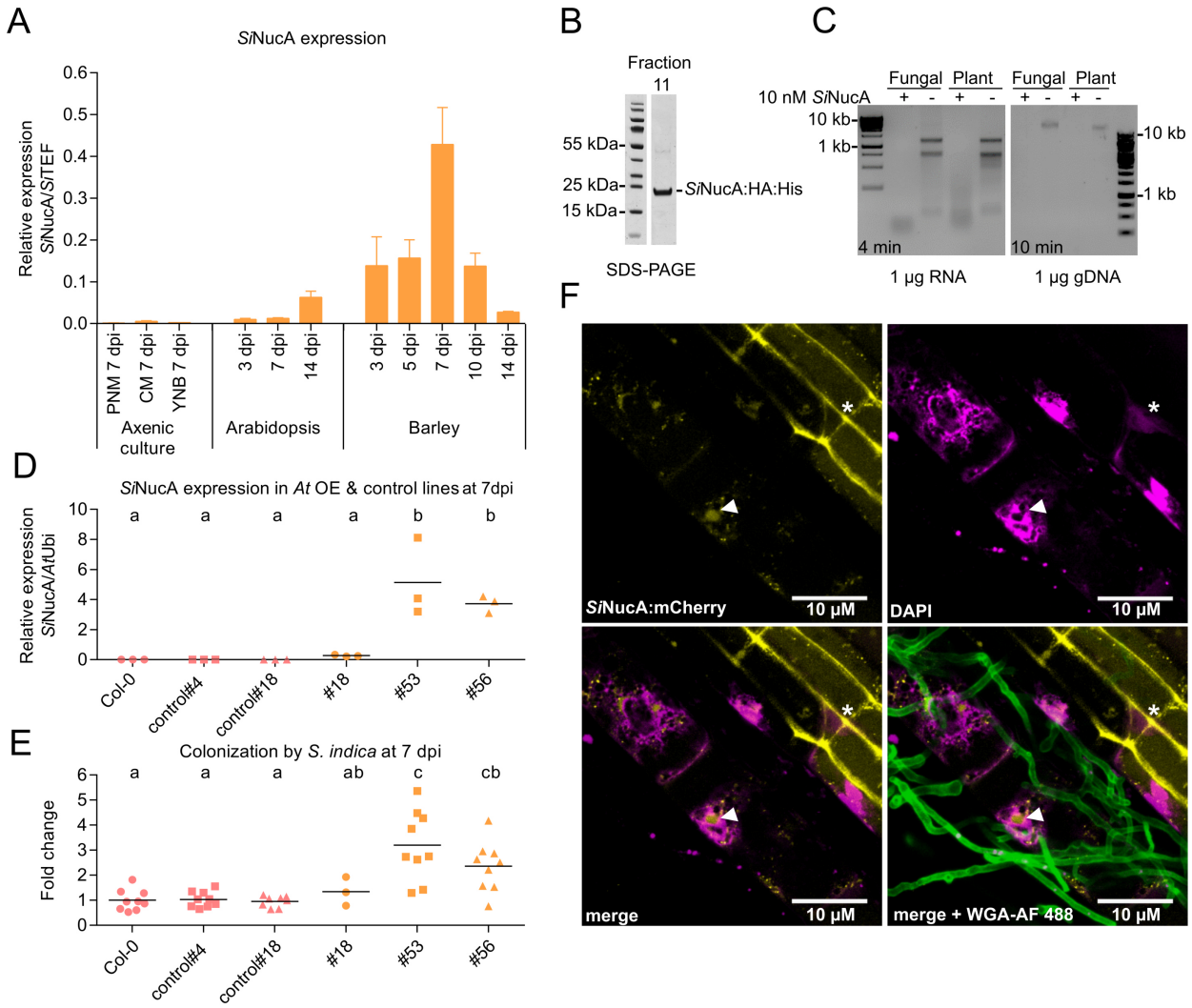

Figure 2. *Si*NucA is a small secreted nuclease involved in fungal accommodation

(A) *Si*NucA expression in *S. indica*-colonized Arabidopsis and barley roots and axenic cultures, measured using the $2^{-\Delta CT}$ method. Error bars: SD, n = 3 (biological replicates).
(B) *Si*NucA:HA:His protein enrichment from culture filtrate precipitated with 80% ammonium sulfate and separated by size exclusion chromatography. The resulting fraction was separated by SDS-PAGE and *Si*NucA:HA:His was stained with Coomassie Blue.
(C) The purified *Si*NucA:HA:His protein was incubated with fungal (*S. indica*) or plant (Arabidopsis) RNA or DNA in 5 mM Tris buffer (pH = 8) with 1 mM $MgCl_2$, and 1 mM $CaCl_2$ for 4 (RNA) or 10 (DNA) minutes and visualized after gel electrophoresis.
(D) Arabidopsis lines expressing *Si*NucA driven by the 35S promoter (lines 18, 53 and 56) compared to control lines (4 and 18: segregating from T2 generation and Col-0 WT). Roots of plants grown on ½ MS medium were inoculated with *S. indica* and analyzed at 7 dpi. Dots represent independent biological replicates, while lines represent the mean. Different letters indicate significant different groups determined with a one-way ANOVA with post-hoc Tukey HSD test ($p<0.05$).

(E) Root colonization by *S. indica* in transgenic 35S::*Si*NucA Arabidopsis lines at 7 dpi was assessed by RT-qPCR comparing the expression of the fungal housekeeping gene *Si*TEF and the plant gene *At*Ubi and the $2^{-\Delta\Delta CT}$ method, normalizing to the Col-0 colonization. Dots represent independent biological replicates, while lines represent the mean. Different letters indicate significant different groups determined with a one-way ANOVA with post-hoc Tukey HSD test ($p<0.05$).

(F) CLSM live cell images of an Arabidopsis root expressing *Si*NucA:mCherry (yellow) inoculated with *S. indica*. Fungal cell walls are stained with WGA-AF 488 (green) and nuclei with DAPI (magenta). *Si*NucA:mCherry accumulates in the apoplast in non-colonized root cells (asterisk) and (re-)localizes to the host nuclei in colonized cells (arrow).

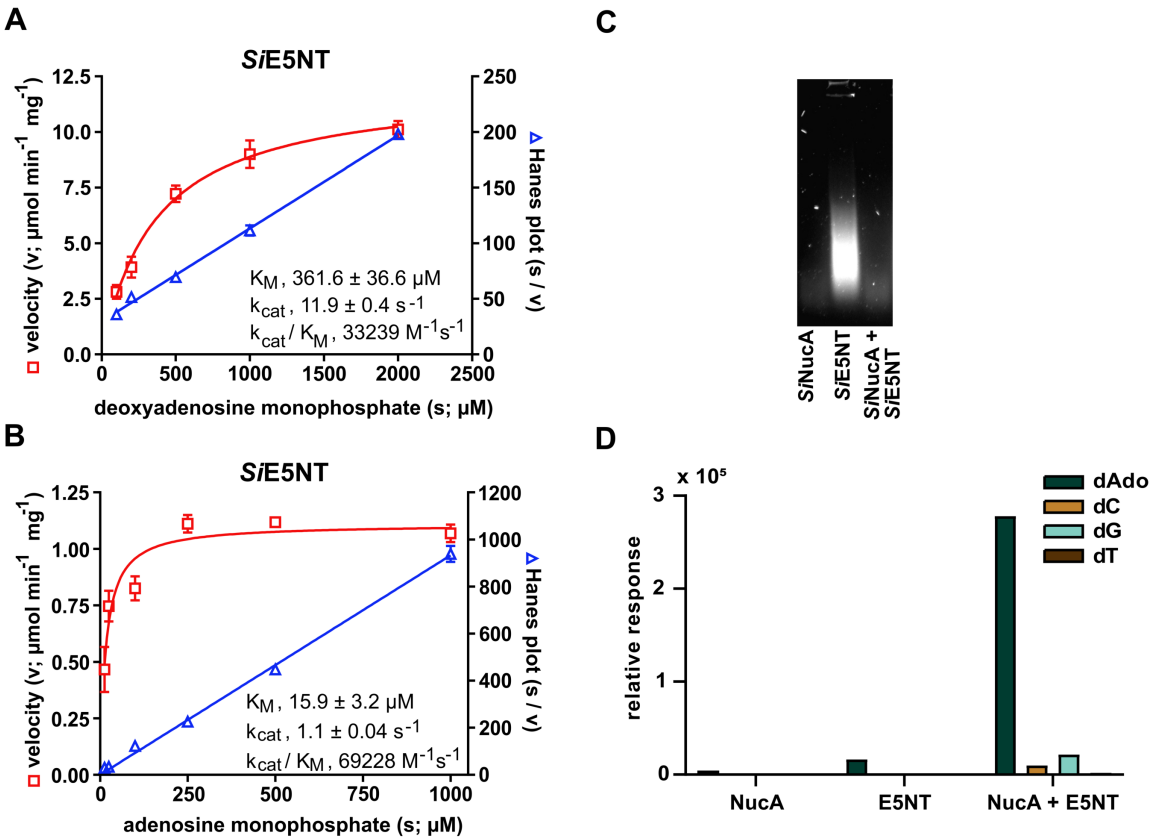

Figure 3. *Si*NucA and *Si*E5NT act synergistically to produce deoxy-nucleosides from DNA

(A) Enzymatic activity and kinetic constants of *Si*E5NT. Left axis, initial catalytic velocity (v) for phosphate production at different dAMP concentrations fitted using the Michaelis-Menten equation. Right axis, ratio of dAMP concentrations and velocities (s/v) plotted against dAMP concentrations (s) fitted by linear regression (Hanes plot). Error bars: SD, n = 3.

(B) Same as in (A) but using AMP as substrate (n = 3).

(C) Degradation of DNA by *Si*NucA and/or *Si*E5NT. 2% agarose gel loaded with the products of an incubation of 10 µg salmon sperm DNA for one hour at 25° C with different

60 enzyme combinations.
61 (D) Relative quantification by HPLC-MS/MS of dAdo (deoxyadenosine), dC (deoxycytidine),
62 dG (deoxyguanosine) and dT (deoxythymidine) released during the incubation shown in
63 (C). Deoxynucleotides could not be detected in any of the reactions.

64

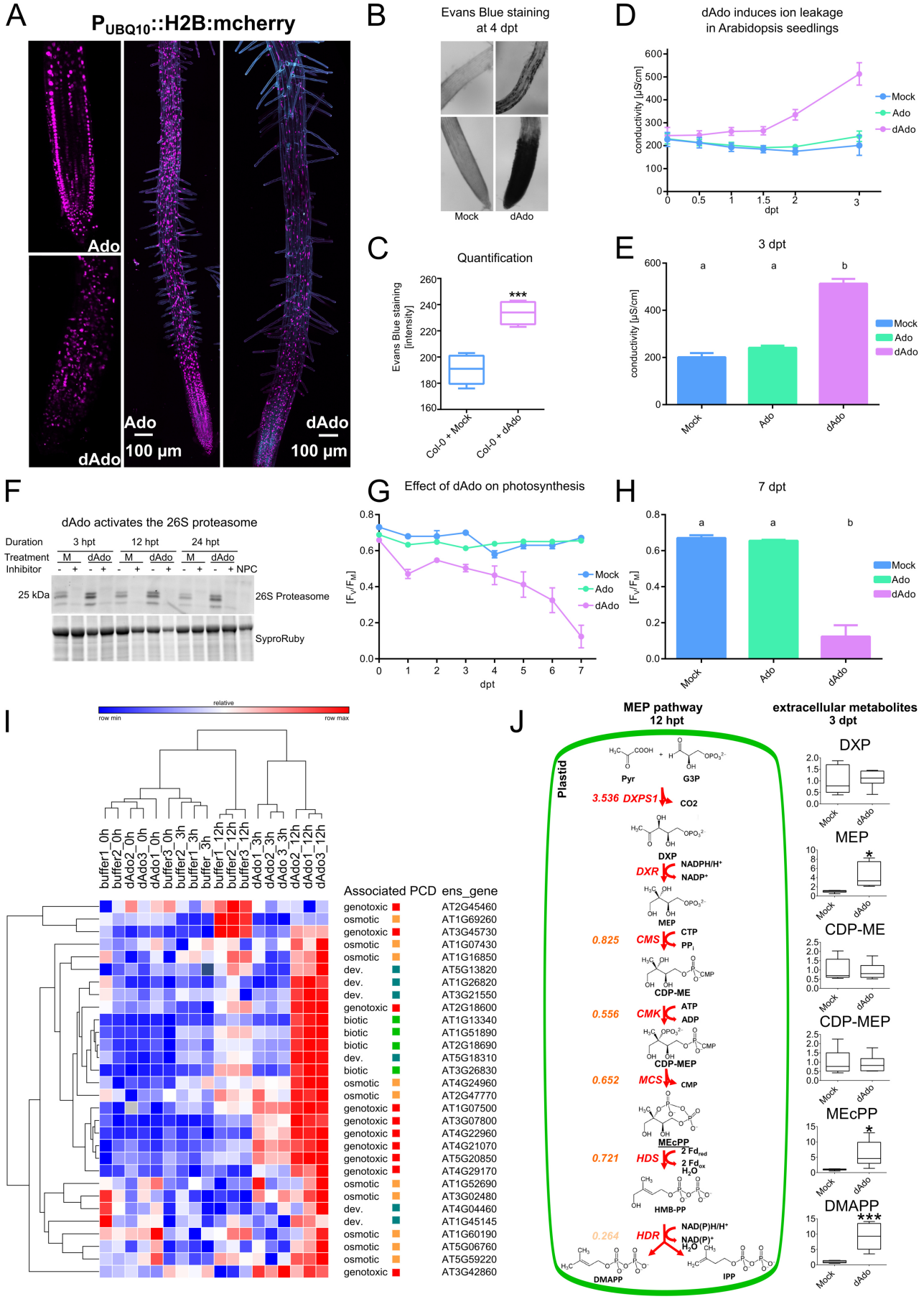
A
P UBQ10::H2B:mcherry
Ado
dAdo
Ado
100 µm
dAdo
100 µm
B
Evans Blue staining at 4 dpt
Mock
dAdo
C
Quantification
Evans Blue staining [intensity]
***
Col-0 + Mock
Col-0 + dAdo
D
dAdo induces ion leakage in Arabidopsis seedlings
conductivity [µS/cm]
dpt
Mock
Ado
dAdo
E
3 dpt
conductivity [µS/cm]
a
a
b
Mock
Ado
dAdo
F
dAdo activates the 26S proteasome
Duration
3 hpt
12 hpt
24 hpt
Treatment
M
dAdo
Inhibitor
NPC
25 kDa
26S Proteasome
SyproRuby
G
Effect of dAdo on photosynthesis
[Fv/FM]
dpt
Mock
Ado
dAdo
H
7 dpt
[Fv/FM]
a
a
b
Mock
Ado
dAdo
I
relative
row min
row max
buffer1_0h
buffer2_0h
dAdo2_0h
dAdo3_0h
dAdo1_0h
buffer3_0h
buffer2_3h
buffer1_3h
buffer_3h
buffer1_12h
buffer2_12h
buffer3_12h
dAdo1_3h
dAdo2_3h
dAdo 3_3h
dAdo2_12h
dAdo1_12h
dAdo3_12h
Associated PCD
ens_gene
genotoxic AT2G45460
osmotic AT1G69260
genotoxic AT3G45730
osmotic AT1G07430
osmotic AT1G16850
dev. AT5G13820
dev. AT1G26820
dev. AT3G21550
genotoxic AT2G18600
biotic AT1G13340
biotic AT1G51890
biotic AT2G18690
dev. AT5G18310
biotic AT3G26830
osmotic AT4G24960
osmotic AT2G47770
genotoxic AT1G07500
genotoxic AT3G07800
genotoxic AT4G22960
genotoxic AT4G21070
genotoxic AT5G20850
genotoxic AT4G29170
osmotic AT1G52690
osmotic AT3G02480
dev. AT4G04460
dev. AT1G45145
osmotic AT1G60190
osmotic AT5G06760
osmotic AT5G59220
genotoxic AT3G42860
J
MEP pathway
12 hpt
extracellular metabolites
3 dpt
Plastid
Pyr
G3P
3.536 DXPS1
CO2
DXP
DXR
NADPH/H+
NADP+
MEP
0.825 CMS
CTP
PPi
CDP-ME
0.556 CMK
ATP
ADP
CDP-MEP
0.652 MCS
CMP
MEcPP
0.721 HDS
2 Fdred
2 Fdox
H2O
HMB-PP
0.264 HDR
NAD(P)H/H+
NAD(P)+
H2O
DMAPP
IPP
DXP
MEP
CDP-ME
CDP-MEP
MEcPP
DMAPP
Mock
dAdo

65

Figure 4. dAdo induces cell death *in planta*

(A) CLSM images of seven-day-old Arabidopsis roots expressing the nuclei marker UBQ10::H2B:mCherry. Incubation with dAdo but not Ado (500 µM) leads to disorganization of Arabidopsis cells in the root tip and to disappearance or fading of the nuclear material.
(B) Bright field microscopy of the root tip and differentiation zone of Arabidopsis seedlings treated with Mock/dAdo (500 µM) and stained with the cell death dye Evans Blue.
(C) Quantification of root cell death in Col-0 root tips at 4 days after dAdo-treatment. Cell death was evaluated using Evans Blue staining. Boxplots represent the data obtained from 5 biological replicates. Asterisks represent significant difference to the Mock-treated sample analyzed by Student's t-test ($p < 0.005$ ***). The experiment was repeated independently 3 times with similar results.
(D) Electrolyte leakage of Col-0 seedlings (9-day-old) in MES buffer after Mock-, Ado- or dAdo-treatment. Error bars depict the standard error of the mean (SEM) obtained from 6 biological replicates. The experiment was repeated independently at least 3 times with similar results. (E) Electrolyte leakage at 3 dpt of the seedlings from (D). Error bars depict the standard error of the mean (SEM) obtained from 6 biological replicates. Different letters indicate significant different groups determined with a one-way ANOVA with post-hoc Tukey HSD test ($p<0.05$). The experiment was repeated independently at least 3 times with similar results.
(F) Activity of the Arabidopsis 26S proteasome. Total protein extracts of 14-day-old seedlings treated with 500 µM dAdo or 2.5 mM MES buffer (M) were incubated with 1 µM of the probe MVB072 (Kolodziejek et al. 2011). Before labeling, samples were incubated with 50 µM of the proteasome inhibitor Epoximycin (+) or DMSO (-). Afterwards, the samples were labeled for 2 hours and separated by SDS-PAGE. The 26S proteasome activity was visualized by fluorescence scanning. SYPRO™Ruby staining was performed to compare sample loads. A non-probe control (NPC) consisting of a mix of all samples incubated with DMSO was used as an additional control. The experiment was repeated twice with similar results.
(G) Photosynthetic activity (F_V/F_M) of 7-day-old Col-0 seedlings incubated with 500 µM Ado or dAdo. Error bars depict the standard error of the mean (SEM) obtained from twelve biological replicates. The experiment was repeated at least 3 times with similar results.
(H) Photosynthetic activity (F_V/F_M) of 7-day-old Col-0 seedlings incubated with 500 µM Ado or dAdo at 7 dpt from (G). Error bars depict the standard error of the mean (SEM) obtained from twelve technical replicates. Different letters indicate significant different groups determined with a one-way ANOVA with post-hoc Tukey HSD test ($p<0.05$).
(I) Heatmap of core regulated cell death (RCD) marker genes expression (selected from Olvera-Carrillo et al., 2015) of 7-day-old Arabidopsis seedlings after dAdo-treatment at 0, 3 and 12 hours. RNA-Seq data are shown as $\log_2$(tpm) (Table S6). Heatmaps and hierarchical clustering (one-minus Pearson correlation) were generated using Morpheus, https://software.broadinstitute.org/morpheus.
(J) Graphical representation of the methyl erythritol 4-phosphate (MEP) pathway. Colored numbers left to key enyzmes represent the $\log_2$ fold-change after 12 hours of dAdo-treatment (Padj < 0.05), measured by RNA-Seq. Boxplots on the right side represent the

corresponding extracellular metabolite levels at 3 dpt. Asterisks represent significant differences to the Mock-treated sample analyzed by Student's t-test ($p < 0.05$ * ; $p < 0.001$ ***).

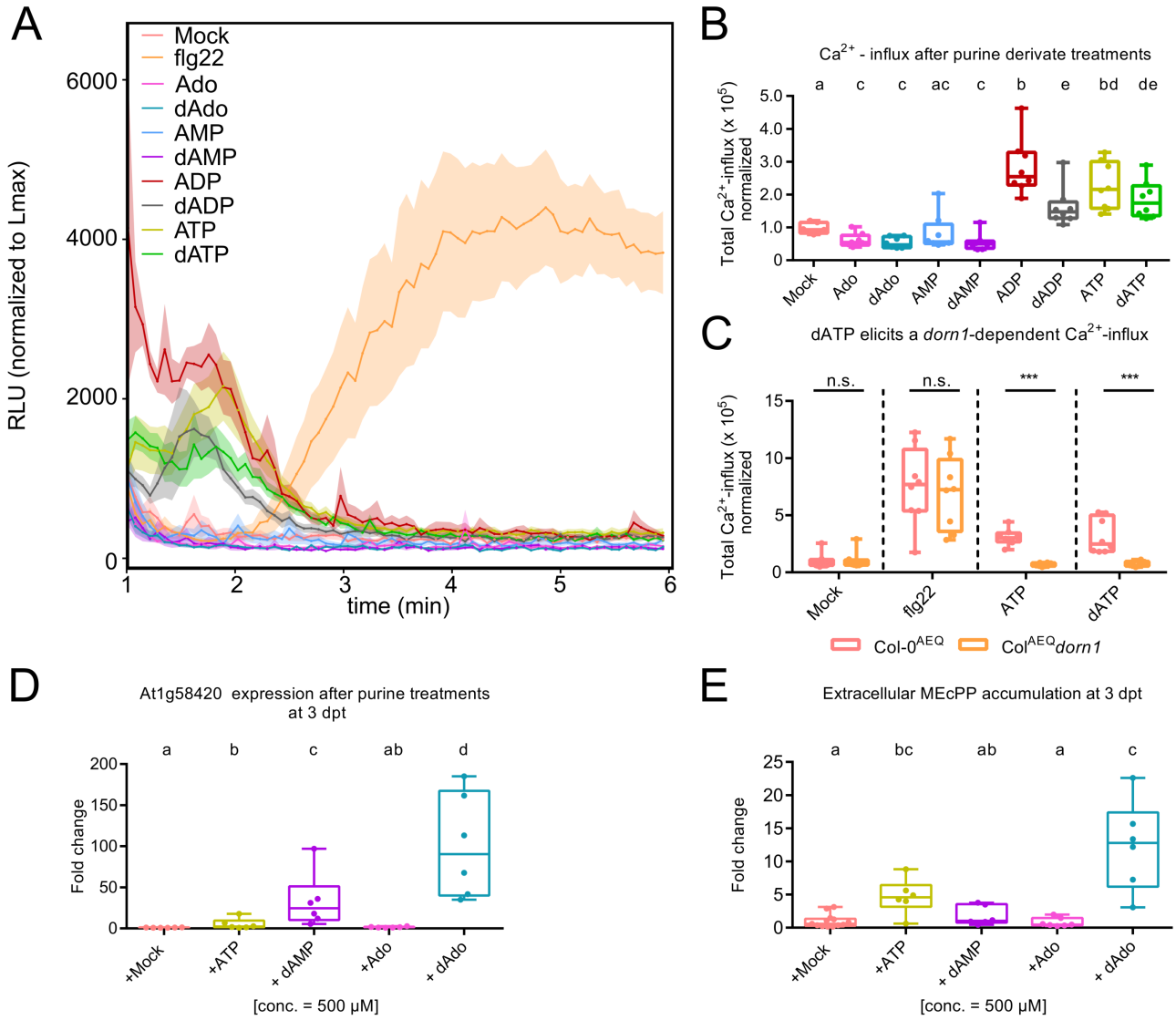

Figure 5. dAdo-triggered signalling and cell death are not mediated by canonical pattern-triggered immune responses

(A) Ca^{2+}-influx after treatment of 7-day-old Arabidopsis Col-0^{AEQ} seedlings with 500 µM purine derivatives solved in 2.5 mM MES buffer (pH 5.7). Buffer and 33 µM flg22 were used as positive and negative controls, respectively. Ca^{2+}-influx was monitored via a coelenterazine-based chemiluminescence assay and measured as relative light units (RLU). After discharging the remaining aequorin by adding $CaCl_2$, discharge kinetics were integrated and normalized to the maximum Ca^{2+} level. The discharge integral was then used to normalize Ca^{2+} kinetics in response to elicitor treatment. Curves represent eight biological replicates and the experiments were additionally repeated independently three times with similar results.

124 (B) Boxplots represent total Ca^{2+}-influx over the measured time period. Calculations were
125 performed as described in (A). Values represent means ± SEM from eight biological
126 replicates, each consisting of one seedling. Different letters indicate significant differences
127 determined by a Kruskal-Wallis test and post-hoc Dunn's test ($p < 0.05$). The experiment
128 was repeated three times with similar results.
129 (C) Comparison of total Ca^{2+}-influx in 7-day-old Arabidopsis Col-0^{AEQ} and Arabidopsis Col-
130 0^{AEQ} *dorn1* seedlings after treatment with 500 µM ATP, dATP, 33 µM flg22 or 2.5 mM MES
131 pH 5.7 (Mock). Data represent values from eight biological replicates. Calculations were
132 performed as described in (A). Asterisks represent significant differences between the two
133 genotypes analyzed by Student's t-test ($p < 0.005$ ***). The experiment was repeated three
134 times with similar results.
135 (D) Expression of the marker gene At1g58420, responsive to wounding and *S. indica*
136 colonization, in treated 7-day-old Col-0 seedlings. Fold change expression was calculated
137 relative to housekeeping gene *At*Ubi and Mock treatment using the $2^{-\Delta\Delta Ct}$ method. Data
138 represents 6 independent biological replicates. Different letters indicate significant different
139 groups determined by Kruskal-Wallis test and post-hoc Wilcox BH adjustment ($p < 0.05$).
140 (E) Metabolic analysis of the supernatant of purine-treated 7-day-old Col-0 seedlings at 3
141 dpt. Dots represent data of at least 6 biologically independent replicates normalized to the
142 average of the corresponding Mock samples. Different letters indicate significant different
143 groups determined by a Kruskal-Wallis test and post-hoc Wilcox BH adjustment ($p < 0.05$).

144

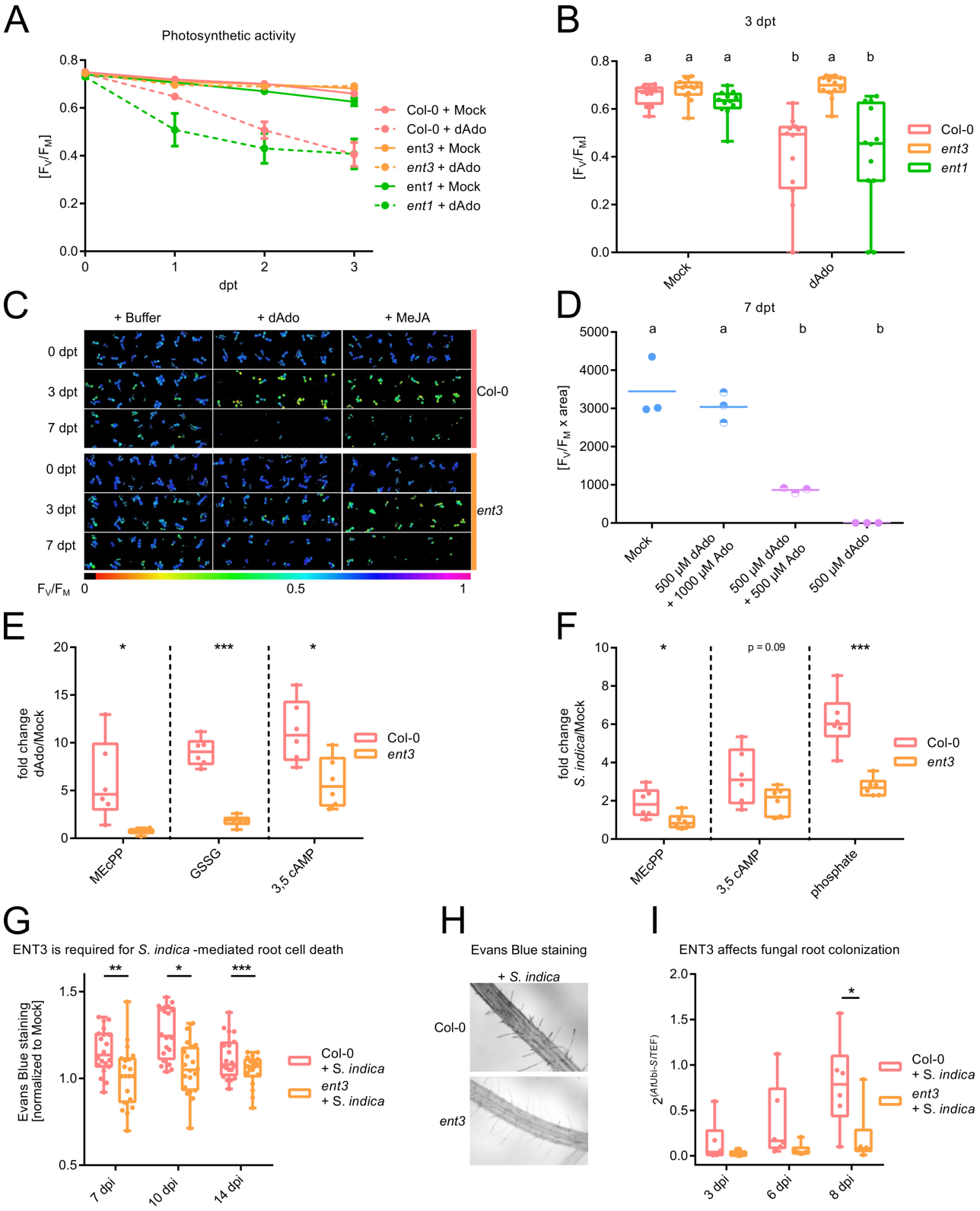

Figure 6. The Arabidopsis equilibrative nucleoside transporter ENT3 is required for dAdo-mediated signalling and cell death

(A) Photosynthetic activity (F_V/F_M) of 9-day-old Mock- and dAdo-treated (500 µM) Col-0, *ent3* and *ent1* seedlings. Measurements were performed 3 days post treatment (dpt), every 24 hours. Data show the mean and error bars depict the standard error of the mean (SEM)

151 obtained from 12 technical replicates consisting of 3 seedlings each. The experiment was
152 repeated more than three times independently, yielding similar results.
153 (B) F_V/F_M of the seedlings from (A) at 3 dpt. Boxplots represent the data of 12 technical
154 replicates consisting of 3 seedlings each. Different letters indicate significant differences
155 determined with a one-way ANOVA with post-hoc Tukey HSD test ($p < 0.05$).
156 (C) Visualization of F_V/F_M measured via PAM fluorometry. The FV/FM value is visualized by
157 the color scale shown below. Depicted are 12 wells containing 9-day-old seedlings,
158 screened at 0, 3 and 7 dpt with either mock treatment (2.5 mM MES buffer pH 5.6), 500 µM
159 dAdo or 500 µM MeJA. The experiment was repeated more than three times independently,
160 yielding similar results.
161 (D) Photosynthetic activity (F_V/F_M x photosynthetically active area) of 9-day-old Col-0
162 seedlings incubated with different concentrations of Ado and dAdo at 7 dpt. Dots represent
163 3 biologically independent replicates consisting of 12 wells containing 3 seedlings each.
164 Different letters indicate significant differences determined with a one-way ANOVA with
165 post-hoc Tukey HSD test ($p < 0.05$).
166 (E) Metabolic analysis of 7-day-old Col-0 supernatants from dAdo-treated and *ent3*
167 seedlings at 3 dpt. Boxplots represent the data of 6 biologically independent replicates
168 normalized to the Mock-treated samples. Asterisks represent significant differences
169 between the two genotypes analyzed by Student's t-test ($p < 0.05$ *,$p < 0.005$ ***).
170 (F) Metabolic analysis of the supernatant from *S. indica*-inoculated 7-day-old Col-0 and *ent3*
171 seedlings at different time points after treatment (3′,5′-cAMP: 3 dpi; MEcPP: 6 dpi;
172 phosphate: 10 dpi). Dots represent the data of 6 biologically independent replicates
173 normalized to the Mock-inoculated samples. Asterisks represent significant differences
174 between the two genotypes analyzed by Student's t-test ($p < 0.05$ (*), $p < 0.005$ ***).
175 (G) Quantification of root cell death in 7-day-old *S. indica*-colonized Col-0 and ent3 roots at
176 7, 10 and 14 dpi. Cell death was evaluated via Evans Blue staining and normalized to the
177 Mock-treated roots. Boxplots represent the data obtained from 20 biological replicates.
178 Asterisks represent significant difference to the Mock-treated sample analyzed by Student's
179 t-test ($p < 0.05$ *, $p < 0.01$ **, $p < 0.005$ ***). The experiment was repeated three times
180 independently, yielding similar results.
181 (H) Evans blue staining of *S. indica*-colonized Col-0 and *ent3* roots at 10 dpi.
182 (I) *S. indica* abundance in 7-day-old Arabidopsis seedlings. The ratio of fungus (*Si*TEF) to
183 plant (*At*Ubi) was calculated using cDNA as template and the $2^{-\Delta CT}$ method. Boxplots
184 represent 6 independent biological replicates. Asterisks indicate significant difference from
185 Col-0 samples (Student's t-test, $p < 0.05$ *).

186

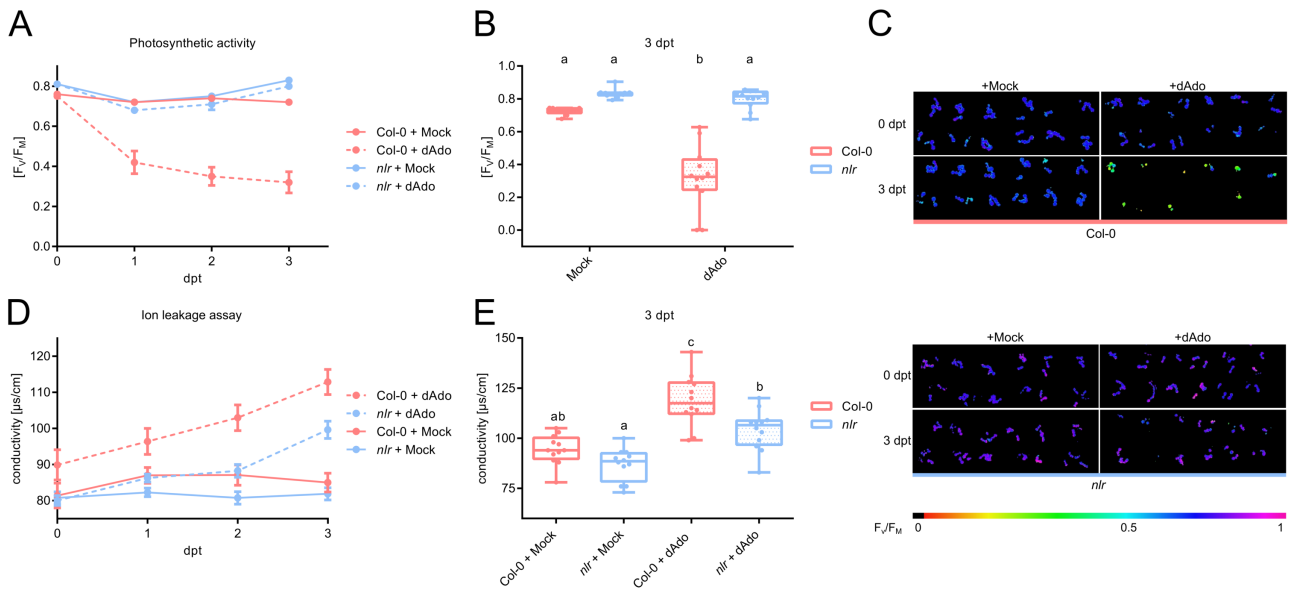

Figure 7. An uncharacterized *At*NLR is involved in dAdo-mediated cell death

(A) F_V/F_M of 9-day-old Mock- and dAdo-treated (500 µM) Col-0 and *nlr* knock-out mutant seedlings. Measurements were performed for 3 days. Data show the mean and error bars depict the standard error of the mean (SEM) obtained from 12 technical replicates consisting of 3 seedlings each. Asterisks indicate significant difference from Col-0 samples (Student's t-test, $p < 0.005$ ***). The experiment was repeated three times independently with similar results.

(B) Boxplots of F_V/F_M measurements from (A) at 3 dpt. Different letters indicate significant differences determined with a one-way ANOVA and post-hoc Tukey HSD test ($p < 0.05$).

(C) Visualization of F_V/F_M measured via PAM fluorometry. Blue indicates a high photosynthetic activity while green decreased and yellow strongly decreased photosynthetic activity. Depicted are 12 wells containing 9-day-old seedlings, screened at 0 and 3 days post treatment (dpt) either with Mock or 500 µM dAdo. The experiment was repeated three times independently with similar results.

(D) Conductivity of MES buffer containing 9-day-old Col-0 or *nlr* seedlings 0 – 3 dpt after Mock- or dAdo-treatment (500 µM). Data points depict the mean, while error bars depict the standard error of the mean (SEM) obtained from 12 biological replicates.

(E) Boxplots of conductivity measurements from (D) at 3 dpt. Different letters indicate significant differences determined with a one-way ANOVA with post-hoc Tukey HSD test ($p < 0.05$).

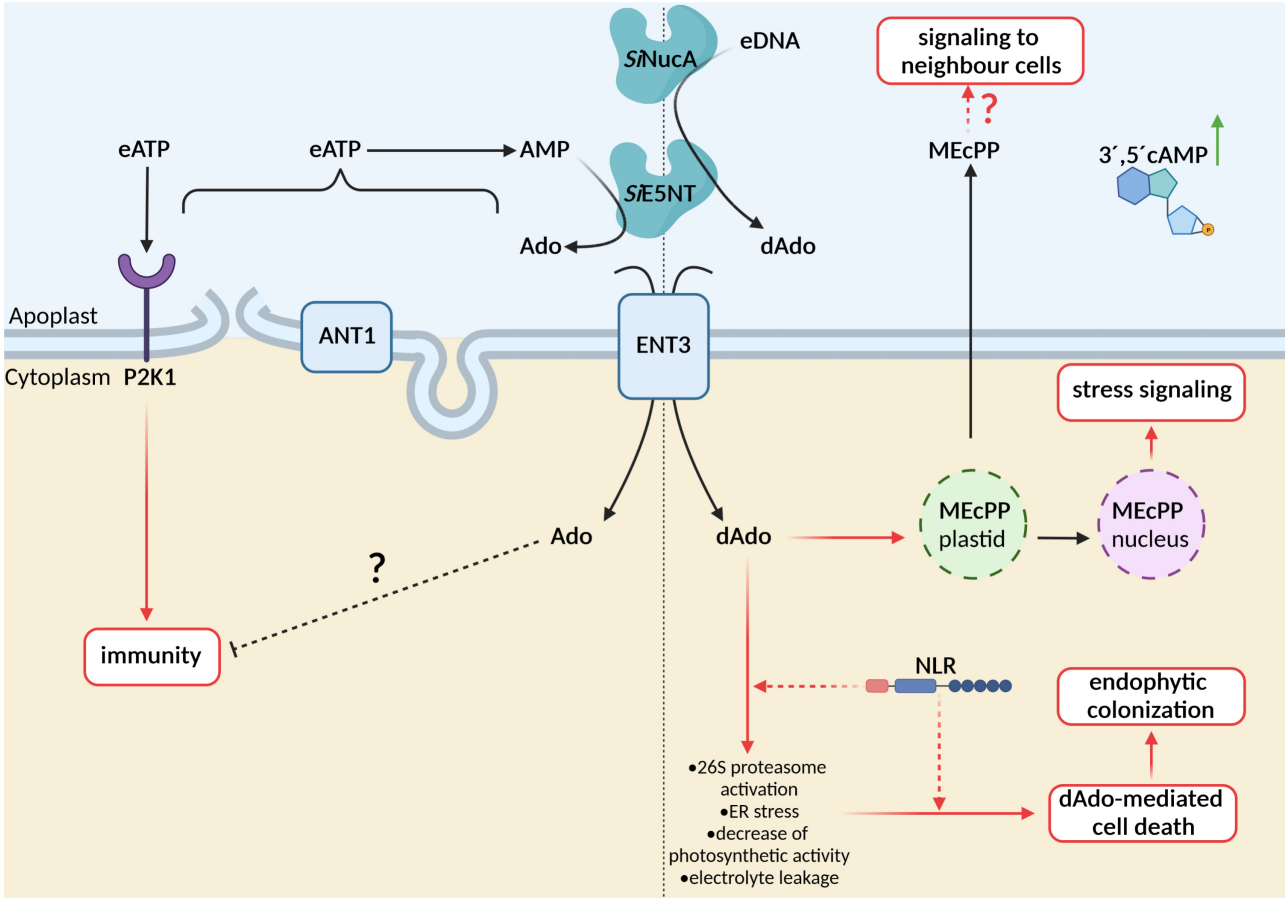

Figure 8. Model for dAdo-triggered cell death during *S. indica* colonization of *A. thaliana* roots

The beneficial endophyte *S. indica* secretes two enzymes into the apoplast, the nuclease NucA and the ecto-nucleotidase E5NT. *Si*E5NT is initially involved in manipulation of the eATP signalling (left side) as described in Nizam et al., 2019. *Si*NucA accumulates at the onset of cell death. The combined activity of *Si*NucA and *Si*E5NT releases deoxynucleosides from DNA with a strong preference for dAdo, a potent cell death inducer in animal systems. dAdo is transported into the cytoplasm *via At*ENT3 where it initiate a cell death process, contributing to successful fungal colonization. dAdo induces production of the retrograde stress signal MEcPP from plastids, activating stress signalling and intercellular communication. dAdo-triggered cell death is modulated by an uncharacterized TR type NLR protein, establishing a link to immunometabolism.